ORSAY

Série A
N° d'ordre : 810

ARTICLE PRINCIPAL

recouvrant en partie la Thèse de Doctorat-ès-Sciences-Physiques

enregistrée au C.N.R.S. sous le numéro A O 5 9 3 6

"INTERPRETATION DES PROPRIETES DES SOURCES D'IONS DU TYPE "DUOPLASMATRON" A PARTIR D'UN MODELE DE LA DECHARGE".

Claude LEJEUNE
Ancien élève de l'E.N.S. de Saint-Cloud
Agrégé de l'Université

Soutenue le 18 Juin 1971 à la FACULTE DES SCIENCES D'ORSAY

devant le jury :

MM. P. GRIVET
G. GAUTHERIN
A. SEPTIER
J.M. DOLIQUE

UNIV.
LEIDEN
BIBL.

NUCLEAR INSTRUMENTS AND METHODS 116 (1974) 417–428; © NORTH-HOLLAND PUBLISHING CO.

THEORETICAL AND EXPERIMENTAL STUDY OF THE DUOPLASMATRON ION SOURCE* PART I: MODEL OF THE DUOPLASMATRON DISCHARGE

C. LEJEUNE

Institut d'Electronique Fondamentale, Laboratoire associé au CNRS, Bâtiment 220, Université Paris-XI, Centre d'ORSAY 91405, France

Received 11 September 1973

The duoplasmatron ion source is extensively used in many domains of experimental physics. In spite of a number of publications about this source, its elementary mechanisms are not yet well understood and no similarity rules are available. These problems have to be solved in order to improve the source properties and to provide the optimum conditions to adapt the extracted ion beam to a device for a particular application.

An exhaustive study of the different plasmas of the discharge has allowed us to explain the physical processes governing the behaviour of the arc with a "dual" compression: geometrically and magnetically; they are discussed briefly. The analysis of the dynamics of the charged particles allows us to propose a one-dimensional static theory of the discharge; its basis and main results – important for the derivation of the source properties — are presented and then compared to experiment and reasonable agreement is observed. Such a model may also be adapted to the magnetized discharge used in certain other ion sources.

1. Introduction

The duoplasmatron as proposed by Von Ardenne offers a number of advantages over existing ion sources: large ion beam intensity, high gas efficiency and capability to produce negative[1]) or multicharged ions[2]). These properties result from the source principle: the ions are axially extracted from the plasma of the low pressure arc between a hot cathode K and an anode A (fig. 1). The emission aperture is bored in the anode, on the discharge axis in the case of positive ion extraction. In order to obtain an enhanced plasma density and a high ionization degree in front of the anode aperture, the discharge is strongly concentrated successively by the focusing action of the intermediate electrode IE and the effect of a strong axial magnetic field set up by the lens, the poles of which are A and IE.

A number of descriptions of the emissive properties of duoplasmatrons with various geometries may be found in the literature. However, the improvement of this extensively used source seems to be more empirical than rational, without relation to the physical processes governing the behaviour of the discharge and the source properties. Thus, owing to the great number of construction and operation parameters, reproductivity and comparison of the results are very difficult. Furthermore, it is impossible to define optimum conditions to adapt the source to a particular application. In order to solve these problems, an experimental and theoretical program directed toward the understanding of charge production and transport mechanism in the discharge, has resulted in the elaboration of a theoretical model of the discharge from which are derived the similarity rules for the duoplasmatron ion source.

This work is a continuation of that done by Demirkhanov and co-workers[3]). The experimental study was a priori very difficult in relation to the intense inhomogeneous magnetic field, the small cross-section diameter ($D \simeq 2$ mm) and the high electron density of the arc plasma ($n_e \simeq 10^{14}$ cm^{-3}). Thus a large scale source was designed to provide[4]):

— a device sufficiently flexible to allow the variation of

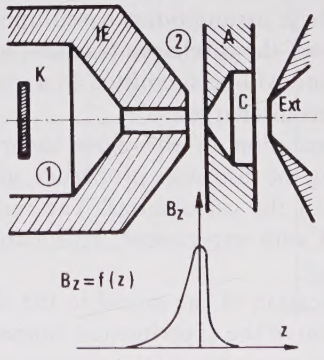

Fig. 1. Schematic diagram of the duoplasmatron structure. (1) Cathode region. (2) Anode region. K — hot cathode; IE — intermediate electrode. A — anode. C — expansion cup. Ext — extractor. $B_{(z)} = f_{(z)}$ — axial profile of the magnetic field, the poles being A and IE.

* The research reported in these papers was sponsored by the CNRS (Centre National de la Recherche Scientifique). It is part of the Doctoral Thesis in Physics presented by C. Lejeune, 18 June, 1971 to the Orsay Centre of the Paris-Sud University and registered by the CNRS under the number AO 5936.

the geometric and magnetic parameters over wide ranges;
— a complete diagnostic of the ionized gas, in particular by means of movable electrostatic probes and by analysis of the radially or axially emitted optical radiation;
— the analysis of mass composition of the emitted ion beam and determination of the energy distribution of the electrons or the ions emitted through the anode aperture[5]).

The mechanism of ion beam formation from a plasma is relatively well understood[6]). With the moderate extraction voltage (30–100 kV) usually applied to the extractor, the dense arc plasma of the duoplasmatron protrudes through the anode aperture. The form of the emissive surface of this "expansion ball" may be shaped in order to improve the ion beam optical properties if the diffusion processes in an "expansion cup" placed just behind the anode are adequately controlled, as previously studied in our laboratory[7]). Thus the emissive properties of the source depend both on the properties of the arc plasma in the plane of the anode aperture and on the diffusion conditions of this plasma in the expansion cup.

This paper and its companion[8]) are mainly devoted to the study of the former problem, and the influence of the expansion cup, which is still being studied, will be published later. Furthermore, because of the complexity of the problem and because we would like to provide a solution as simple as possible, which will be useful for the non-plasma physicist, we restrict ourselves to the following points:
— A brief description of the main processes which govern the evolution of the "dual" confinement arc, and of the assumptions of the model of the discharge. The theoretical and experimental justifications of these assumptions, based upon an exhaustive study of the discharge plasmas, are developed in ref. 4 and will be submitted to a journal specializing in gas discharges.
— The presentation of the main theoretical results concerning the discharge properties, giving only the principle of the calculations. The results are then compared with experiment; reasonable agreement is observed.
— The application of the model to the theoretical interpretation of the experimental emissive properties of the source: ion beam intensity and mass composition, ionization efficiency and energy distribution. The similarity rules of the duoplasmatron ion source are then derived. This latter point is developed in part II of the present article[8]).

2. Physical mechanisms of the discharge

In a previous paper[9]) we described the experimental variations of the emissive properties of the duoplasmatron ion source in relation to the two principal regimes of the constricted arc discharge. The main results were as follows. When the source geometry is fixed, as a first approximation, the emissive properties depend only on three independent parameters: the arc current I_A, the magnetic field maximum B and the pressure p_A in the anode chamber. The arc changes from "normal mode" for lower values of arc current to "starvation mode" as the neutral density inside the arc column decreases. This decrease results from the high ionization efficiency when arc current increases. Furthermore, the regime-change-over point is characterized by the following properties:
— $I_A \cdot p_A^{-1} B^\alpha = \text{const.}$ (α depends on the geometry $\alpha \simeq 1/2$)
— The floating potential of the IE (related to the grounded anode) is close to the value of potential corresponding to the maximum value of the single ionization cross section of the gas.
— The ion beam intensity and the ionization efficiency are maximum, the latter being close to unity.
— The mean ion energy depends mainly on the nature of the gas.

These characteristics as well as the variation of the properties in each mode are qualitatively explained by the physical mechanisms occurring in the discharge. They were deduced from the complementary analysis of the ionized gas parameters by mean of electrostatic probes and of the energy distribution of the charges emitted through the anode aperture[5]). These data also furnish the description of the different plasmas of the arc and the axial variation of density and potential, discussed below.

2.1. The geometric constriction sheath

In the normal arc mode, the geometric constriction as now understood involves the presence of an electrostatic double layer and thus a potential discontinuity at the cathode side of the IE canal[10]). This sheath connects two plasmas: the "quasi-cathode" plasma from which is extracted an electron flux I_e and the "quasi-anode" plasma from which is extracted an ion flux I_{+1}. As the electric field at the plasma boundaries is approximately zero, these flux are space-charge limited and have to satisfy the stability criterion derived by Langmuir[11]):

$$I_e/I_{+1} = (M/m)^{1/2}, \qquad (1)$$

where M and m are respectively the ion and electron

masses. The creation of such a sheath is necessary to insure both the arc conduction and the space-charge neutrality through the discharge compression. These conditions may be satisfied by the choice of two main parameters of the layer: its shape in the quasi-cathode plasma and the height of its potential discontinuity.

— The position of the sheath fixes the electron flux I_e extracted from the "quasi-cathode" plasma. As seen from eq. (1), the ion flux is smaller than the electron flux, the latter being almost equal to the arc current I_A in the "quasi-anode" discharge.
— Its potential jump causes an increase of the ionization rate in the "quasi-anode" plasma and thus, according to the transport conditions, fixes the ion flux I_{+1} coming back to the sheath. This flux has to satisfy eq. (1).

In the duoplasmatron, as the intermediate electrode is conducting, the geometric constriction layer connects the plasmas of two discharges: the cathode discharge between the cathode and the IE; and the anode discharge between the cathode plasma and the anode.

The intensity of these discharges may vary independently by the variation of the IE bias; generally the IE is floating and the two discharges have almost the same arc current[8]).

2.2. The cathode discharge

The cathode discharge is a classical diode type arc; the electron emission from the hot cathode, governed by an electrostatic double layer, may be either space-charge or temperature limited[12]). The arc conduction is insured by an almost equipotential plasma, the ionization being mainly due to a Maxwellian electron population. The electron temperature T_{e_1} corresponds to that predicted by the theories of positive columns ($T_{e_1} \simeq 2$ eV with a pressure of 10^{-1} torr of argon). The potential V_{p_1} of the cathode plasma relative to the grounded anode depends only on I_A, B and p_A. When the arc is far from its regime-change-over point the anode pressure is the most sensitive parameter, the potential being more negative as the pressure decreases.

At the wall of the IE an ion space-charge monolayer is formed having a potential jump which is fixed in order to satisfy the boundary conditions of the cathode discharge. If the IE is floating, electron and ion flux are equal, and its potential V_{IE} is mainly fixed by the more negative plasma of the arc, i.e. the cathode plasma (V_{p_1}), by a relation similar to that derived for electrostatic probes[13]):

$$V_{p_1} - V_{IE} \simeq \frac{kT_{e_1}}{2e} \log\left(\frac{2}{\pi}\frac{M}{m}\right). \qquad (2)$$

Thus the variation of V_{IE} follows the variation of the cathode plasma potential V_{p_1}, the former being slightly more negative ($\simeq 10$ V in argon) than the latter. This remark is useful in order to allow a rapid determination of the operation mode of a duoplasmatron with a given gas.

2.3. The anode discharge in the normal mode

2.3.1. *Electron emitter and arc conduction*

The anode discharge is supplied with electrons extracted from the cathode plasma by the potential jump in the sheath. These "primary" electrons travel throughout the anode plasma without evidence of anomalous randomization resulting from collective interaction — a phenomenon known as "Langmuir's paradox" [14]). The presence of these energetic electrons has been detected up to the plasma-jet emitted through the anode aperture[5]). This particularity is a consequence of the following facts:

— The electron beam is initially focused by the concave sheath and the electric forces in the plasma, and then, because of the small incidence angle of the electron trajectories, the particle reflection in the magnetic mirror is negligible. Therefore, the electron beam is channeled by the magnetic field lines within a flux tube.
— The beam losses due to scattering on the neutrals are weak, because for the usual pressure in the anode chamber, the thermalization length is much larger than the discharge length. It results that the energetic electron beam insures most of the arc con-

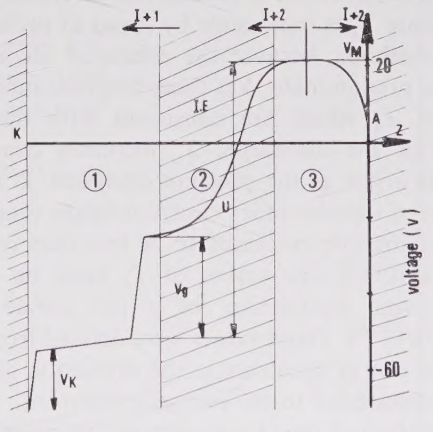

Fig. 2. Schematic profile of the potential along the discharge axis in the normal arc mode. (1) Cathode plasma. (2) Intermediate plasma. (3) Anode column. V_k — cathode fall. V_g — potential jump in the constriction sheath. V_M — "negative" anode fall. eU — energy of the primary electrons. I_{+2} — ion flux at the anode column ends. I_{+1} — ion flux at the sheath boundary.

duction in the anode plasma. Thus this plasma differs from a classical positive column in which the arc conduction is insured by the thermal electrons. In particular, the reduction of the arc cross section in the magnetic constriction does not involve the creation of a new double layer as was generally believed[15]). This would occur in a positive column as the axial mobility of thermal electrons is greatly reduced by the magnetic field-line convergence[3]). Therefore, in the normal arc mode, there is an axial gradient of electron density and potential, as verified by probe data, between the magnetically confined plasma which we name the "anode column" and the "intermediate plasma" situated in the IE canal (fig. 2).

On the other hand, if the diameter of the IE canal is too large compared to the cathode chamber diameter there is no double layer at the canal entrance; the arc conduction in the "intermediate plasma" is then due to thermal electrons and a double layer appears in the region of the maximum axial gradient of the magnetic field. Under these conditions, the anode column properties differs from those of the normal mode column; they may be compared to the properties observed in the "arc starvation" mode (section 2.4).

2.3.2. *Production and axial transport of the charges*

In the anode column the energetic electron beam has a high current density ($j_e \simeq 500$ A cm^{-2}). This insures an intense charge production rate by a Townsend-α mechanism. The high value of the self-collision frequency of the secondary electrons causes their thermalization. However, a precise measurement of their temperature T_e is impossible by mean of probes or by optical methods, because the effects of the energetic electrons predominate. Yet these methods furnish estimates of T_e which are consistent with the energy balance of the discharge; T_e increases from about 3–6 eV in argon as the pressure decreases[4]). The contribution of the secondary electrons to the total ionization may then be evaluated to be less than one third. These relatively low values of T_e must be opposed to the usual assumption of a hot anode plasma ($T_e \simeq 20$ eV)[16]). Those values were derived from analysis of the energy spectrum in the extraction space and thus corresponded to the energetic electrons.

The motion of the charges across the magnetic field lines is greatly reduced as compared to the axial motion: the charges have to escape axially. As the electron axial mobility is higher than the ion mobility, an excess of positive charges is set up and thus a potential maximum appears between the anode and the magnetic constriction. Following an analysis of the equilibrium conditions of a discharge, as proposed by Kliarfeld and Neretina[17]), the potential maximum is necessary in the duoplasmatron arc. It has two effects:

— It traps the secondary electrons and modifies their flow in order to satisfy the continuity condition on the anode. It is a "negative anode fall".

— It accelerates the ions both toward the anode and toward the constriction sheath in order to satisfy its stability criterion.

The study of the anisotropy of the charge energy distribution in the anode column has verified directly the existence of the "potential hill". Its position does not correspond to the axial maximum of the magnetic field but to the middle plane of the anode column[4]).

2.3.3. *Radial distribution of plasma density*

It is possible to distinguish two main regions in the anode column, in the radial direction: a bright core corresponding to the region where the primary electron beam is confined and a dark diffusion-type plasma.

Near the axis the radial distributions of electron density n_e may be fitted to a Gaussian curve:

$$n_{e_{(z,r)}} = n_{e_{0_{(z,0)}}} \exp\left[-(r/\beta)^2\right], \tag{3}$$

where z defines the axial position of the arc cross section and r is the radial distance from axis. In the case of an unsaturated magnetic circuit the "radius" β of the Gaussian profile ($\beta \simeq 1$ mm) and the maximum electron density satisfy the empirical relations:

$$n_{e_{0_{(z,0)}}} \sim B_{(z)}, \tag{4}$$

$$\beta^2_{(z)} \times B_{(z)} \simeq \text{const.} \tag{5}$$

Thus the anode column plasma is confined within a flux tube as is the electron beam which insures its creation.

In the diffusion plasma ($r \geqslant 3\beta$) the electron density decreases exponentially with an e-folding length q, the value of which is about five times the ion gyroradius ($q \sim B^{-1}$). The motion of the charges across the magnetic field is due to the associated effects of the ion gyroradius and of the guiding centre distribution[4]). These effects prevail over a collisional diffusion mechanism and there is no evidence of "drain diffusion" as long as the arc is in the normal mode.

2.3.4. *Ion flux to the geometric constriction sheath*

As the ion flux I_{+2} issued from the "anode column" goes through the intermediate plasma, it loses particles

before reaching the geometric constriction sheath (intensity I_{+1}) as the result of interactions with neutrals and walls. The importance of the interaction with neutrals is proved by the strong neutral pressure gradient which exists between the cathode and the anode chambers when the discharges operates[4]). The ratio $\gamma = I_{+1}/I_{+2}$ may be evaluated experimentally and will be considered as a secondary parameter of the model.

2.3.5. *Conclusion*

In summary, the anode discharge equilibrium mechanisms are related as follows (fig. 2):

— When the primary electrons extracted from the cathode plasma (potential V_{p_1}) reach the anode column (potential V_M), their kinetic energy eU is

$$eU = e(V_M - V_{p_1}).$$

— The ionization rate in the anode column is mainly related to the value of this kinetic energy and to the value of the neutral density (Townsend-α process).

— The ion flows I_{+2} across each end of the anode column are equal. Their intensity I_{+2} results from the balance between charge production and loss.

— When reaching the geometric constriction sheath, the ion flux issued from the anode column is reduced to a value $I_{+1} = \gamma I_{+2}$ as a result of the losses in the IE plasma. This flux must then satisfy the sheath stability criterion [eq. (1)].

The determination of the energy eU of the primary electrons results from this diagram, and thus the potential difference between anode column and cathode plasma. Then the potential V_M of the former, related to the grounded anode, is fixed from the continuity condition on the anode, the "negative anode fall".

Therefore, if γ is taken as a parameter, the theoretical axial distribution of potential along the discharge may be derived from the theoretical analysis of the processes occurring in the magnetically confined anode column.

2.4. The anode discharge in the arc starvation mode

The important influence of the anode pressure on the variation of the energy eU appears clearly in the previous diagram. When the neutral density in the arc column decreases, the energy eU must increase. If it reaches the value eU_M corresponding to the ionization cross-section maximum, any further decrease in neutral density is incompatible with the stability of the geometric constriction layer and the arc mode changes. In particular, a reorganization of the distribution of the ion guiding centres appears in the anode column which blows up (fig. 3). This new distribution results from the formation of a double layer in the magnetic constriction, in the region of the maximum gradient of the axial magnetic field. Thus the primary electrons travel through the magnetic mirror. They are responsible for the ionization in the core of the arc. A large fraction of the electrons extracted from the intermediate plasma by the sheath is reflected on the magnetic mirror, the incidence angle of their trajectories being greater than that of the loss cone of the mirror. Furthermore, they oscillate in the potential well created between the anode and the magnetic constriction sheath. These electrons are responsible for the ionization in the plasma surrounding the core and for the "anomalous radial diffusion" observed under these conditions of arc starvation.

These new mechanisms are correlated with an increasing level of the noisy instabilities of the discharge[18]). They may be compared to those occurring in a PIG-discharge where the hindered radial motion of the electrons involves such instabilities and "drain-diffusion[19]).

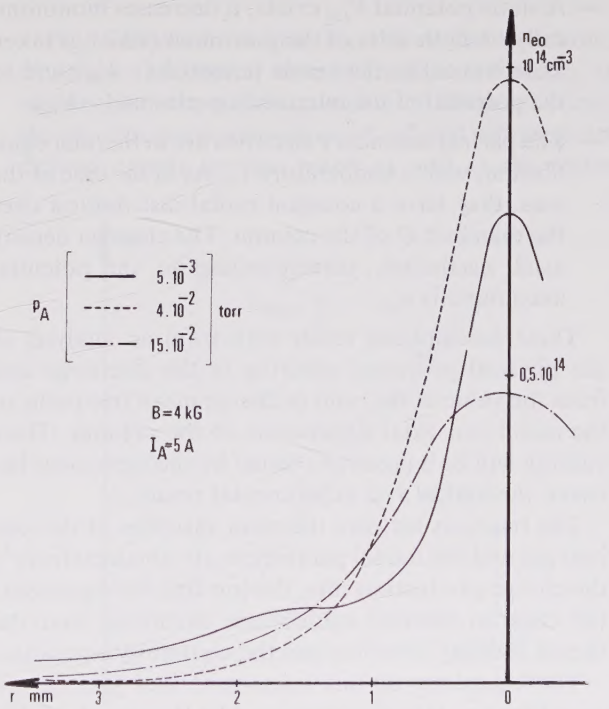

Fig. 3. Experimental variation of the electron density as a function of the radial distance from the discharge axis — anode pressure parameter. For the lower pressure the arc runs in the starvation mode; gas: argon.

3. Theoretical model of the discharge

3.1. The assumption of the "anode column" model

In order to solve the problem of the emissive properties of the duoplasmatron with axial extraction from a plasma in which the charge radial motion across the magnetic field are greatly reduced as compared to the axial motion, we define the following linear model:

— The magnetic field is uniform along the z axis over a distance L equal to the "anode column" length.

— The primary electrons are monoenergetic (eU) and have an axial velocity. Their radial distribution is constant over a cross section of the column, the diameter being D. The electron losses are weak, and are characterized by the fraction K of the total intensity entering the column.
Singly-charged ions of mass M are generated with a uniform rate per unit volume per second and with a zero initial velocity. They drift axially to the ends of the column without collisions (free-fall approximation).

— The neutral density n is constant inside the column. As a result of the ionization it differs from the density n_0 outside the column.

— A static potential $V_{(z)}$ exists; it decreases monotonically on both sides of the maximum (which is taken as reference) to the anode potential $(-V_M)$ and to the potential of the intermediate plasma $(-V_B)$.

— The plasma secondary electrons are in thermal equilibrium, with a temperature T_e. As in the case of the ions, they have a constant radial distribution over the diameter D of the column. The electron density axial maximum, corresponding to the potential maximum, is n_{e0}.

These assumptions result both from an analysis of the physical processes occuring in the discharge and from the value of the ratio of charge mean free paths to the radial and axial dimensions of the column. Their validity will be a posteriori tested by the agreement between theoretical and experimental results.

The relations between the main variables of the ionized gas and the model parameters are obtained from[4]) the charge-production rate, the ion free-fall equations, the electron thermal equilibrium equations, and the sheath stability criterion and the continuity equations.

The equations of this beam-generated plasma are issued from a static theory derived by Dunn and Self[20]). This theory requires only minor modifications of the Langmuir—Tonks free-fall theory of the positive column.

3.2. Theoretical results

We report only those which are necessary for the interpretation of the source properties without details of the calculations.

3.2.1. *Properties independent of the neutral pressure*

It is interesting to note that, whereas the neutral pressure strongly affects the potentials in the discharge, it does not modify certain properties of the discharge such as the ion flux to each column ends

$$I_{+2} = I_A \times \left(\frac{m}{M}\right)^{1/2} \times \frac{1}{\gamma}; \tag{6}$$

and thus the intensity of the ion beam emitted through an anode aperture of diameter d

$$I_+ = I_A \times \left(\frac{m}{M}\right)^{1/2} \times \frac{1}{\gamma} \times \left(\frac{d}{D}\right)^2; \tag{7}$$

and the axial maximum of the electron density

$$n_{e0} = \frac{4I_A}{0.4\,e\pi D^2} \times \frac{1}{\gamma}\left(\frac{m}{2kT_e}\right)^{1/2}. \tag{8}$$

This density varies slightly with the pressure owing to the corresponding variation of the temperature T_e.

3.2.2. *Existence of the regime-change-over point*

i) *Mean neutral density* n *in the anode column*

To obtain the total ionization rate R_+ in the column we first derive the ionization probability P of the neutral flux Φ_0 entering the electron beam:

$$P = R_+/\Phi_0 = 1 - \exp\left[-\frac{I_A \sigma \chi}{eD}\left(\frac{2M}{\pi k T_0}\right)^{1/2}\right]. \tag{9}$$

In this relation σ is the ionization cross section, T_0 is the neutral temperature and χ is a correcting factor for thermal ionization ($\chi \simeq 3/2$). We write this expression in the simplified form

$$P = 1 - \exp(-a), \tag{9'}$$

where a is called the ionization index. We then calculate R_+ independently by the usual expression[21])

$$R_+ = I_A \sigma \chi n L/e. \tag{10}$$

Comparison between eqs. (9) and (10) gives

$$n = n_0\left(\frac{1 - \exp(-a)}{a}\right). \tag{11}$$

This relation shows the decrease of the neutral den-

sity in the column when the ionization index increases as a result of arc current growth.

ii) *Neutral density minimum* n*

To satisfy the sheath criterion, the probability P must more over be equal to

$$P = \frac{I_A}{en_0\gamma DL}\left(\frac{8m}{\pi kT_0}\right)^{1/2} \leqslant 1. \qquad (12)$$

As P is smaller than unity, eq. (12) defines the theoretical minimum value n_0^* of the neutral density outside the column which is compatible with the existence of a normal arc mode when arc current, magnetic field and geometry are fixed. We obtain:

$$n_0 \geqslant n_0^* = \frac{I_A}{e\gamma DL}\left(\frac{8m}{\pi kT_0}\right)^{1/2}. \qquad (13)$$

As n_0 tends to n_0^* all neutrals entering the electron beam are ionized ($P = 1$), the ionization index becomes infinite [eq. (9′)] and the neutral density in the column tends to zero [eq. (11)]. In fact, a practical limitation to these variations occurs in relation to the existence of a maximum value σ_M for the ionization cross-section of the gas. The electron energy is then eU_M, which is a gas characteristic parameter. These limits are:

$$a \leqslant a_M = \frac{I_A\sigma_M\chi}{eD}\left(\frac{2M}{\pi kT_0}\right)^{1/2}, \qquad (14)$$

$$n \geqslant n^* = \frac{2}{\gamma\sigma_M\chi L} \times \left(\frac{m}{M}\right)^{1/2}. \qquad (15)$$

Only the geometry and the gas affect the n^* value which is the minimum of the neutral density inside the column. It is obtained when the ionization probability is maximum, its value being

$$P_M = 1 - \exp(-a_M). \qquad (16)$$

The neutral density outside the column is then, from eq. (11):

$$n_0'^* = n^*\left(\frac{a_M}{1 - \exp(-a_M)}\right) \geqslant n_0^*. \qquad (17)$$

Thus, if the pressure outside the column is constant ($n_0 = n_0'^*$), eqs. (14) and (17) define a maximum value I_{AM} for the arc current. Any further increase of arc current is incompatible with the ionization and transport mechanisms of the normal mode. These mechanisms have to be physically modified. The arc changes from "normal to "arc starvation" mode. It is clear from eqs. (14) and (17), that the same phenomenon occurs if, the arc current being fixed, the neutral density outside the column decreases.

iii) *Maximum arc current in the normal mode*

The maximum arc current as calculated from eqs. (14) and (17) corresponds in fact to arc starvation (i.e. P close to unity), if the ionization index a_M is large enough [eq. (16)]. From eq. (17) and fig. 4, it is clear that this occurs if the regime-change-over point is obtained under conditions where the neutral density outside the arc $n_0'^*$ is much larger than n^*. The maximum arc current is then

$$I_{AM} \simeq en_0 DL\gamma(\pi kT_0/8m)^{1/2}, \qquad (18)$$

which valid if $n_0 \geqslant 3\, n^*$.

Moreover it appears from eq. (17) that a normal arc mode may only operate if $n_0 \geqslant n^*$. Thus n^* is the absolute minimum of gas density in the anode compartment compatible with the existence of any arc operating in the normal mode.

3.2.3. *Variation of the primary electron energy*

The primary electron energy eU is obtained from the set of eqs.:

$$\begin{cases} \sigma = f(U): \text{ gas ionization cross section}, & (19) \\ \sigma = \left(\dfrac{m}{M}\right)^{1/2} \times \dfrac{2}{\gamma\chi Ln}. & (20) \end{cases}$$

Fig. 5 shows for argon, the theoretical variation of U versus the neutral density outside the arc n_0 and versus the corresponding value n of the density inside the arc. The particular values n^*, n_0^* and $n_0'^*$ previously defined appear on this graph as well as the regime-

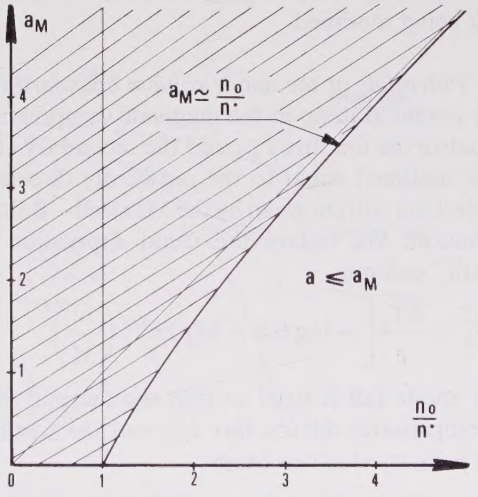

Fig. 4. Maximum possible value of the ionization index as a function of the normalized neutral density: ratio of the neutral density n_0 outside the arc to the absolute minimum of gas density n^*.

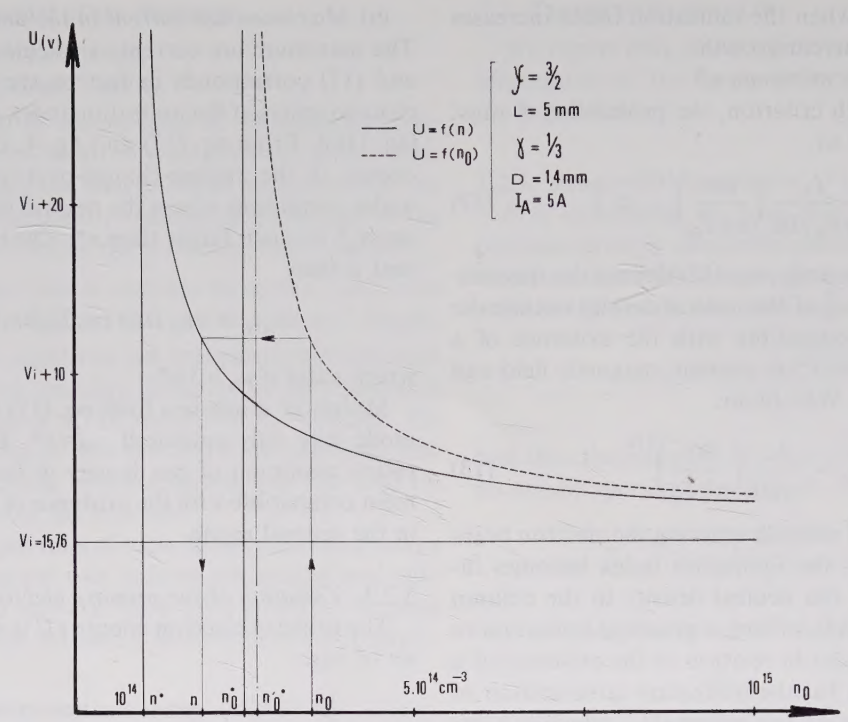

Fig. 5. Calculated variation for argon of primary electron energy as a function of neutral density n_0 outside the arc column and as a function of corresponding value n of the neutral density inside the column. When arc starvation occurs: $n \rightarrow n^*$ and $n_0 \rightarrow n_0'^*$; n_0^* is the theoretical minimum density corresponding to an ionization probability equal to unity. V_i is the ionization threshold of the gas.

change-over point (in relation to the decrease of the neutral density n and to the maximum of the ionization cross section).

Fig. 6 shows the same phenomenon as the arc current increases, the geometric parameters of the column L and D being modified.

3.2.4. *Potentials at the anode column boundaries*

The potential jump in the magnetic compression has to equalize the ion flux I_{+2} and the secondary electron escape, assumed equal to the outwardly directed random electron current given by the Maxwell—Boltzmann distribution. We obtain the usual expression for a "freefall" column

$$V_B = \frac{kT_e}{e}\left[-\log 0.4 - \log 2\pi^{1/2}\left(\frac{m}{M}\right)^{1/2}\right]. \quad (21)$$

The anode fall is fixed so that the thermal electron flux compensates the ion flux I_{+2} and the weak losses of the primary electron beam

$$V_M = \frac{kT_e}{e}\left\{-\log 0.4 - \log 2\pi^{1/2}\left[\left(\frac{m}{M}\right)^{1/2} + \gamma K\right]\right\}. \quad (22)$$

The strong influence of the secondary electron temperature appears in these relations, as γK has only a slight influence (because of the logarithm). Thus the potential at the boundaries will depend mainly on the pressure and on the gas. For argon their values are:

$$V_B \simeq 5.2\,\frac{kT_e}{e} \quad (23)$$

$$2.4\,\frac{kT_e}{e} < V_M < 3.6\,\frac{kT_e}{e}, \quad \text{if} \quad \frac{1}{15} < \gamma K < \frac{1}{60}. \quad (24)$$

4. Experimental results

As previously noted, the analysis of probe data in the discharge plasmas and the analysis of charge extracted beam through the anode hole permit the experimental evaluation of the secondary parameters of the model as well as the spatial variation of electron density and plasma potential.

We present here the more important results.

4.1. Secondary parameter variations

Table 1 summarizes as a first approximation the secondary parameter variations which have been mea-

TABLE 1

Independent parameters	Secondary parameter variations for a normal mode	Modification after regime-change-over point	Range of variation
I_A (0–20 A)	γ independent of I_A, B, p_A	γ increases	1/6–1/3
B (0–10 kG)	L independent of I_A, B, p_A	L, constant	2–15 mm
p_A 10^{-2}–10^{-1} torr	D { independent of I_A; $D=2\beta\sim B^{-1/2}$; increases slowly as p_A increases }	D, increases	1–10 mm
	K { independent of I_A; decreases as B increases; increases slowly as p_A increases }	K, increases slightly	1/10–2/10

Note: The Gaussian radial variation of electron density is normalized to a rectangular profile, the density of which is equal to the maximum density of the Gaussian profile. As a result the column diameter is equal to 2β and varies as $B^{-1/2}$ if the magnetic circuit is unsaturated (no change in field topography) [eq. (5)].

sured for various electrode geometries and magnetic field topographies as a function of the independent parameters.

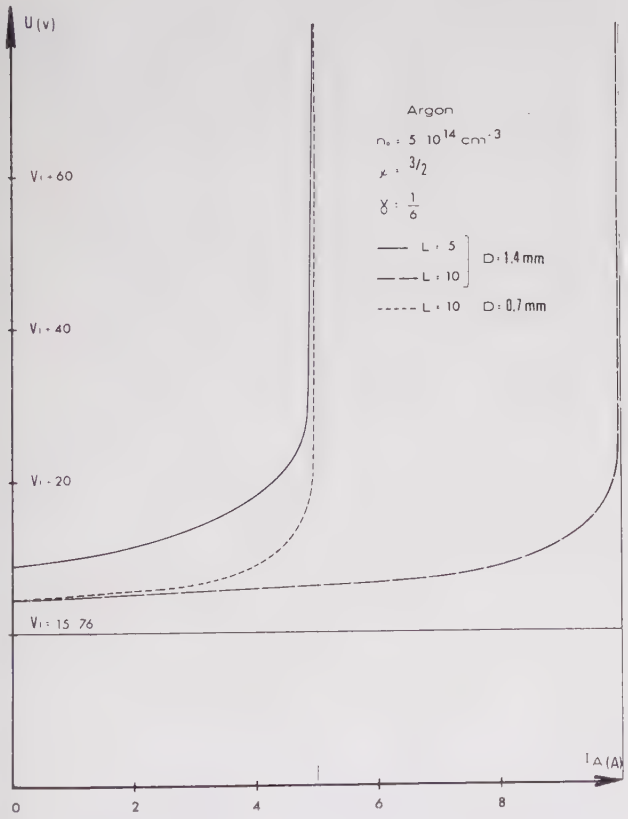

Fig. 6. Calculated variation of primary electron energy as a function of arc current for argon; anode column length and diameter arc parameters.

4.2. THE REGIME-CHANGE-OVER POINT

4.2.1. *Influence of the source geometry*

According to the source geometry the arc mode changes either continuously or discontinuously. A particular case illustrating these two possibilities is shown in fig. 7, the anode extraction hole being either on the discharge axis or one millimeter off-axis. In the former case the arc column length may adjust itself in a small range by the plasma expansion in the extraction space and the arc changes progressively to starvation mode. On the contrary, if the column boundary is well defined on the anode, one notes: a jump of the cathode plasma

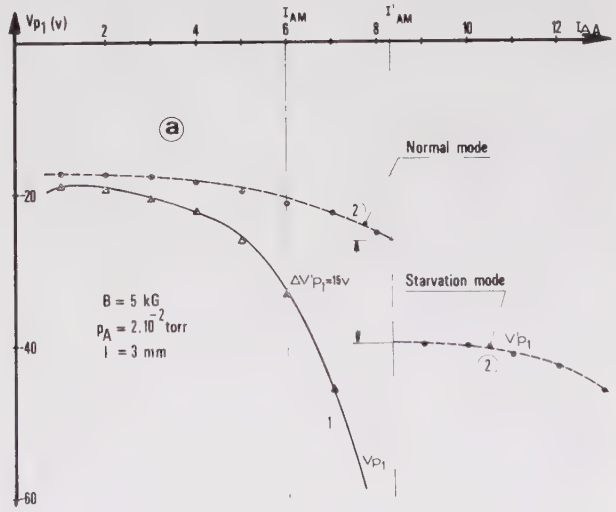

Fig. 7. Variation for argon of the cathodic plasma potential V_{p_1} as a function of arc current — dependence on the source geometry. (1) The anode aperture is on the discharge axis. (2) The anode boundary is on the anode plane. A discontinuity exists between the two possible modes of the arc.

TABLE 2

Independent parameters	Secondary parameters	I_{AM} theoretical [eq. (18)]	I_{AM} experimental
$B = 5$ kG	$\gamma \simeq \frac{1}{3}$		on-axis anode hole $I_{AM} \simeq 6$ A
$p_A = 2.10^{-2}$ torr $l = 3$ mm (argon) (distance between A and IE)	$D \simeq 1.4$ mm $L \simeq 5$ mm	$I_{AM} = 10$ A	off-axis hole $I_{AM} = 8.4$ A

potential (about 15 V) related to the creation of the new sheath; and a slight increase of the maximum arc current, which results from the ionization of the re-emitted neutrals after ion recombination on the anode, the effect of which has been neglected in the model.

These observations are a test of validity of the proposed mechanisms when arc starvation occurs. Usual values of the arc parameters (conditions of fig. 7) are reported in table 2 where a fair agreement is noted between experimental and theoretical values of the maximum arc current, taking account of the complexity of the problem. For the case where the arc mode changes continuously, the regime-change-over point is found from the maximum of extracted ion current.

4.2.2. *Relations between independent parameters*

The variation of the maximum arc current as a function of the anode pressure is shown in fig. 8 for three different values of the distance l between the anode and the IE. This distance is modified without variation of the magnetic field topography by changing the thickness of a molybdenum disk supported by the iron anode. In this condition, the experimental values of the parameters γ and D are independent of l, whereas the column length L is given by the empirical relation:

$$L \simeq l + 2 \text{ mm}.$$

In fair agreement with the prediction of eq. (18), the

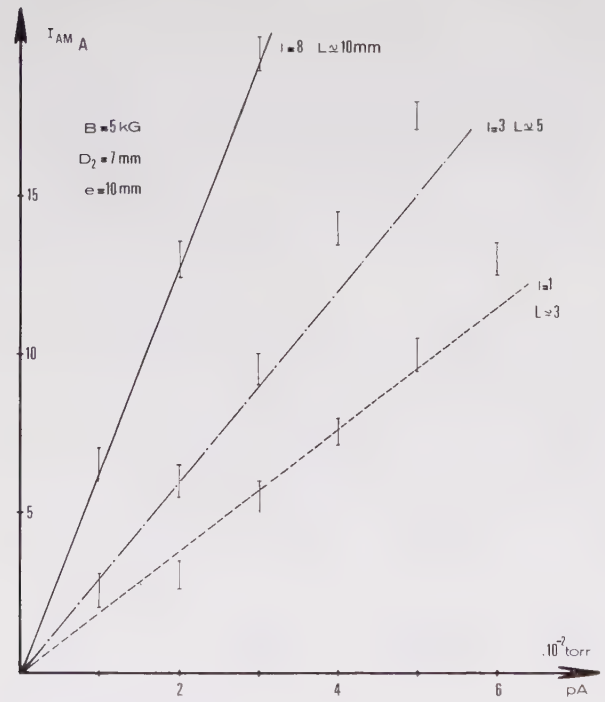

Fig. 8. Dependence of the maximum arc current I_{AM} on the anode pressure for three values of the distance l between the A and the IE. L is the corresponding measured value of the anode column length. The distance $e = 10$ mm between the magnetic poles is constant. ($D_2 = 7$ mm is the IE canal diameter.)

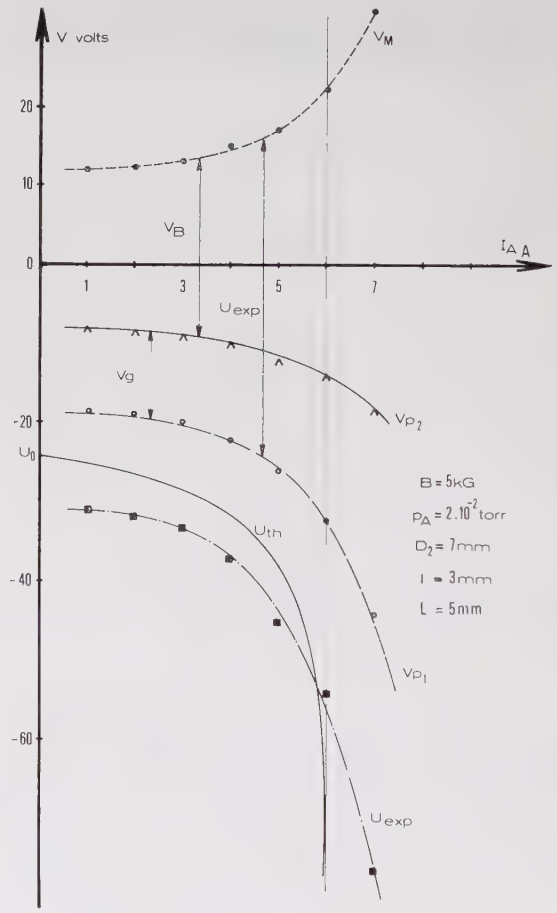

Fig. 9. Comparison of theoretical (U_{th}) and experimental (U_{exp}) variation of primary electron energy with arc current. The experimental value is obtained from the values V_{p_1} and V_M of the cathode plasma and anode column potentials. V_{p_2} is the intermediate plasma potential.

maximum arc current is proportional to the column length whereas the slight divergence from linearity versus pressure is related to the slight variation of the column diameter.

The influence of the magnetic field has also been studied. We may conclude that in the case of an unsaturated magnetic circuit, when the regime-change-over point of the arc is obtained, the main parameters of the source satisfy the empirical relation:

$$I_{AM} \times B^{1/2} \times p_A^{-1} \times L^{-1} \simeq \text{const.} \qquad (25)$$

This relation is in agreement with the theoretical prediction deduced from eq. (18) and from the variation of the secondary parameters reported in table 1. The value of the constant in eq. (25) depends slightly on the IE canal, the magnetic field topography and the nature of the gas. Its variation lies within a factor two. Further experimental results are discussed in part II[8]).

4.3. The potentials in the discharge

Fig. 9 gives the experimental variations versus arc current of the respective potential V_{p_1}, V_{p_2}, V_M of the cathode, intermediate and anode plasmas. The variation of the primary electron beam energy has been dededuced from those values and compared to the theoretical variation calculated from eqs (19) and (20). The value of $\gamma(\gamma = 1/5)$ used for this comparison has been chosen in order to fit the experimental and theoretical value of I_{AM}. The agreement is satisfactory, and is conserved when the discharge parameters are modified. For instance, the influence of the gas on the primary electron energy is shown in fig. 10. These variations agree with the model, in particular the value U_M when starvation occurs lies within a range of values, dependent on the source geometry, which corresponds to the maximum of the ionization cross section for formation of monocharged ions.

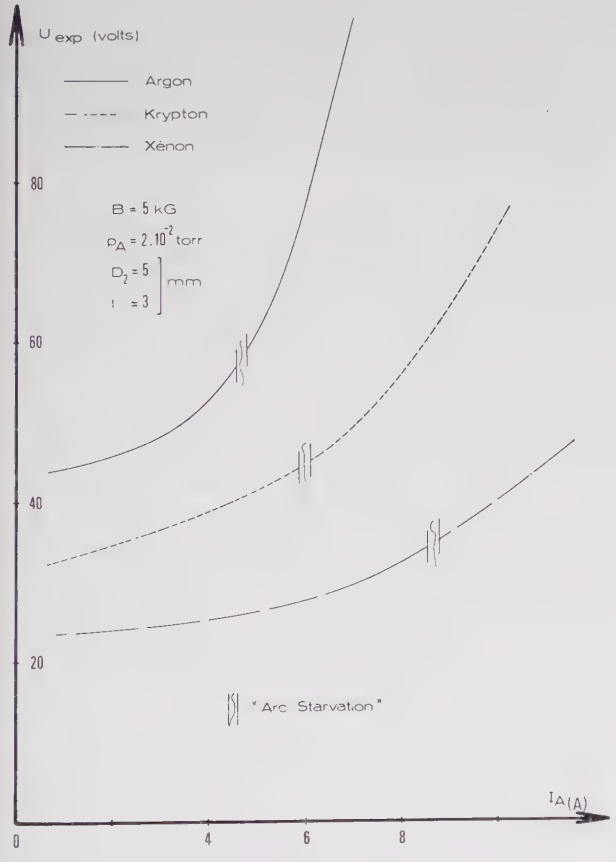

Fig. 10. Experimental dependence of primary electron energy on the nature of the gas.

As the secondary electron temperature T_e in the anode column may not be measured accurately (section 2.3.2), a thermal equilibrium has been assumed between the electrons in the anode column and in the IE plasma; the temperature T_{e_2} of the latter is measured with electrostatic probes[4]). Its value is related to the value of the primary electron energy and as a first approximation we may propose the empirical relation

$$kT_e \simeq kT_{e_2} \simeq eU/10, \qquad (26)$$

which is consistent with the energy balance of the anode discharge. If such a value of the electron temperature is adopted in eqs. (23) and (24), the calculated values of the potentials V_B and V_M at the anode column boundaries are in agreement with the experimental values.

5. Conclusion

The results of the one-dimensional model we have derived from the analysis of the duoplasmatron discharge mechanisms are in reasonable agreement with the experimental results. In particular, a quantitative interpretation of the arc current limitation is given — a phenomenon very important owing to its influence on the ion source properties.

Such a model in spite of its necessary approximations in relation with the inhomogeneous magnetic field, is useful because:

It describes the properties of a dense steady-state ionized column which may be used as an electron beam plasma amplifier or as an active medium of an ionic laser cavity[4]).

It also allows the derivation of the similarity rules of the duoplasmatron ion sources. In particular, it will provide a basis for the study of the discharge instabilities which strongly affect the ion beam focus. Further-

more, it has been shown that, in the case of a finite cylinder, the steady state of a magnetized discharge has separable solutions for the radial and axial dependence of plasma density, potential and charge velocities[22]). Thus a radial model of the discharge may be separately elaborated from the previous described mechanisms. Such a model is necessary in order to derive the properties of the duoplasmatron source with off-axis-extraction which has been shown to be a very convenient source for negative ion beam formation[1]).

Finally, it may be adapted to the magnetized discharges used in ion sources such as calutron, hollow cathode or PIG sources.

It is a pleasure to acknowledge many fruitful discussions with Prof. G. Gautherin and the expert assistance of A. Chabrier with the experimental program. The author is indebted to Dr. A. Schlachter who has taken much trouble in improving the english in this paper.

References

1) M. Dubarry and G. Gautherin, Proc. 1st Intern. Conf. *Ion Sources* (Saclay, 1969) p. 133.
2) H. Krupp, Nucl. Instr. and Meth. **90** (1970) 167.
3) R. A. Demirkhanov, H. Fröhlich, V. V. Kursanov and TT. Gutkin, B.N.L. Report **767** (1962) 218.
4) C. Lejeune, Doctorat Thesis, no 810 (Orsay, 1971).
5) G. Gautherin, C. Lejeune and A. Septier, Plasma Physics **11** (1969) 397.
6) A. Septier, *Focusing of charged particles* vol. II, (Academic Press, New York, 1967) chap. 3.4, p. 123.
7) G. Gautherin, Doctorat Thesis, (Orsay 1967).
8) C. Lejeune, Part II of this article, Nucl. Instr. and Meth. **116** (1974) 429.
9) C. Lejeune, Proc. Symp. *Ion sources and formation of ion beams*, B.N.L. 50310 (Brookhaven 1971) p. 27.
10) M. J. Schönhuber, Proc. 3rd Intern. Conf. *Phenomena in Ionized Gases* (Venice 1957) p. 930.
11) J. Langmuir, Phys. Rev. **33** (1929) 945.
12) L. Malter, E. O. Johnson and W. M. Webster, R.C.A. Rev. **12** (1951) 415.
13) F. F. Chen, *Plasma Diagnostic Techniques*, (eds. R. H. Huddlestone and S. L. Leonard; Academic Press, (1965) chap. 4, p. 112.
14) E. W. Crawford and S. A. Self, Int. J. Electr. **18** (1965) 569.
15) H. Fröhlich, Nucleonik **1** (1969) 183.
16) J. Kistemaker, P. K. Roland and J. Politiek, Nucl. Instr. and Meth. **38** (1965) 1.
17) B. N. Kliarfeld and N. A. Neretina, Sov. Phys. Tech. Phys. **28** (1958) 271.
18) C. Lejeune, Proc. 2nd Intern. Conf. *Ion Sources* (Vienna, 1972) p. 387.
19) A. V. Zharinov, Plasma Phys. **1** (1960) 267.
20) D. A. Dunn and S. A. Self, J. Appl. Phys. **35** (1964) 113.
21) T. L. Hill and L. H. Aller, in *Characteristics of Electrical Discharges in Magnetic fields* (eds. A. Guthrie and R. K. Wakerling; McGraw Hill, New York, 1949), chap. 8, p. 166.
22) D. B. Ilić and S. A. Self, Stanford University Institute for Plasma Research, S.U.I.P.R., Report no. 446, (1971).

NUCLEAR INSTRUMENTS AND METHODS 116 (1974) 429–443; © NORTH-HOLLAND PUBLISHING CO.

THEORETICAL AND EXPERIMENTAL STUDY OF THE DUOPLASMATRON ION SOURCE*

PART II: EMISSIVE PROPERTIES OF THE SOURCE

C. LEJEUNE

Institut d'Electronique Fondamentale, Laboratoire associé au CNRS, Bâtiment 220, Université Paris-XI, Centre d'ORSAY 91405, France

Received 11 September 1973

The theoretical variations of the properties of the ion beam extracted from a duoplasmatron source are derived from a model of the discharge and then compared with experiment. Satisfactory agreement is observed for the influence of the operating parameters as well as for that of the geometric parameters on the ion beam intensity, the ion beam composition, and the ionization efficiency; similarity rules of the source are derived. From these results, the optimum parameters of the source may be determined, according to the requirements of any particular application.

1. Introduction

In a previous paper[1]), hereafter referred to as Part I, we proposed a theoretical model of the low pressure discharge operating in a duoplasmatron ion source. The conclusions of the model are in agreement with the experimental variations of electron density and potential along the discharge axis. It is likely that these variations determine the variations of the emissive properties of the source with axial extraction of the charged particles through the anode hole, in particular the ion beam intensity, the mass and charge composition of the beam, the ionization efficiency and the ion energy spectrum. These properties, as well as the optical quality of the ion beam, are affected by the extraction conditions. The influence of the polarization of the expansion cup placed just behind the anode has already been studied[2]).

From a practical point of view, it is useful to separate the influence of the expansion cup from the influence of the main discharge. Thus the purpose of this paper, is the study of the properties of the plasma jet emitted through the anode aperture of the duoplasmatron, as functions of the construction and operation parameters of the source. The experimental results are compared to the theoretical variations derived from the discharge model. Satisfactory agreement is observed; a unified description of the variation of the emissive properties is given in relation to the two possible modes of the discharge. The operation near the regime-change-over point of the arc is particularly interesting: the beam intensity and the ionization efficiency are maximum. Quantitative expressions describe the source properties. They are the similarity rules for the duoplasmatron source. Such rules are necessary in order to obtain a logical improvement of the source performance because (1) the number of source parameters is large (see table 1 and fig. 1), and (2) the requirements of the source are quite different according to its specific application. It is well known that the duoplasmatron is extensively used both in fundamental and applied physics.

The results presented in this paper concern, for the sake of simplicity, the positive ions of noble gas. The emission aperture is bored in the anode on the discharge axis. Details about experimental methods for beam composition and beam energy spectrum analysis have been reported previously[3,4]). The particular conditions for hydrogen positive and negative ion extraction can be found in work performed in our laboratory[5]).

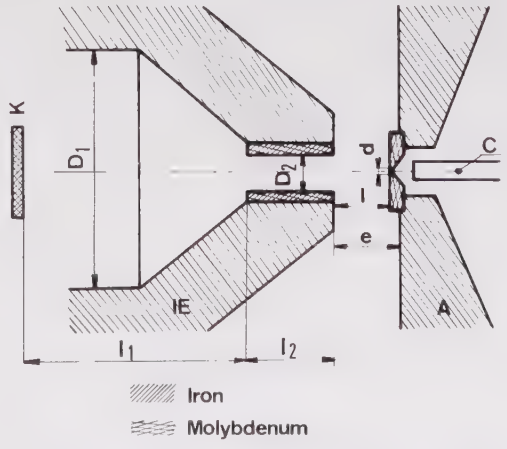

Fig. 1. Schematic diagram of duoplasmatron structure and geometric parameters (see table 1). K — cathode; IE — intermediate electrode; A — anode; C — collector.

* The research reported in this paper was sponsored by the CNRS (Centre National de la Recherche Scientifique). It is part of the Doctoral Thesis in Physics presented by C. Lejeune, 18 June, 1971 to the Orsay Centre of the Paris-Sud University and registered by the CNRS under the number AO 5936.

TABLE 1

The main parameters of the duoplasmatron ion source (see fig. 1).

	Range of variation
Geometric parameters	
— l : distance between A and IE	1–15 mm
— l_2 : length of the IE canal	10–40 mm
— D_2 : diameter of the IE canal	5–10 mm
— D_1 : diameter of the cathode region	80 mm
— l_1 : distance from K to the IE canal	50–100 mm
— d : diameter of the emission aperture	0.3–1 mm
Magnetic parameters	
— B : axial maximum of the magnetic field topography	0–10 kG
— e : distance between magnetic poles.	
Electric parameters	
— I_A . arc current (c.w. operation)	0–20 A
— V_A : arc voltage	0–200 V
— V_{IE} : IE potential (the anode is grounded)	0–200 V
— P_C : cathode heater power	30–100 W
— V_{ext} : extraction voltage	0–30 kV
Pressure parameters	
— p_K : pressure in the K region	10^{-2}–7.10^{-1} torr
— p_A : pressure in the A region	10^{-2}–10^{-1} torr
— N_0 : neutral flow	4.10^{-4}–4.10^{-3} cm³·atm·s^{-1}
Gas parameters	
— M : ion mass	
— T_0 : neutral temperature	500 K
— σ_M } maximum of the	
— U_M } ionization cross section	
Model parameters	
— L : length of the anode arc column	$L \simeq l+2$ mm
— D : diameter of the anode arc column	$D \sim B^{-1/2}$
— γ : coefficient for ion losses in the IE canal	1/6–1/3
— K : coefficient for electron losses in the anode column	0.1–0.2
— T_e : secondary electron temperature	3–7 eV

2. Emitted ion beam intensity

2.1. THEORETICAL EXPRESSIONS

The ions emitted through the anode aperture are those created in the anode column from the potential maximum to the anode and then transported towards the anode by the action of the plasma electric field. From the free-fall theory of the plasma[6]) the ion current density j_+ at the plasma-sheath boundary is related to maximum of the electron density n_{e_0} by the equation:

$$j_+ = 0.4\, e n_{e_0} (2kT_e/M)^{1/2}. \tag{1}$$

We note that this expression is similar to that obtained by Bohm[7]) for the ion collection by an electrostatic probe. Furthermore, to satisfy the stability criterion of the geometric constriction sheath[1]), the ion current density at both ends of the anode column is related to the primary electron beam density j_e by:

$$j_+ = j_e (m/M)^{1/2} \gamma^{-1}. \tag{2}$$

Thus the ion beam current through an anode aperture of diameter d is given by:

$$I_+ = I_A (m/M)^{1/2} (d/D)^2 \gamma^{-1}, \tag{3}$$

where the influence of multiply-charged ions as well as the influence of the radial variation of electron density have been neglected. This latter contribution may be evaluated from the Gaussian profile of electron density, in the anode column (Part I, section 2.3). From eq. (3) (Part I) and eq. (1) above one obtains:

$$I_+ = I_A \left(\frac{m}{M}\right)^{1/2} \frac{1}{\gamma} \left[1 - \exp\left(-\frac{d}{2\beta}\right)^2\right], \tag{4}$$

where β is the e-folding distance from the axis of the Gaussian profile. For the case where $d \ll 2\beta = D$, eq. (4) reduce to eq. (3).

The duoplasmatron may also be used as an electron source. The electron flow through the anode hole contains two populations which are created in two different regions of the discharge; thus their kinetic energy differs. The primary electrons which are issued from the cathodic plasma have an intensity

$$I_e = I_A (1-K)(d/D)^2. \tag{5}$$

The secondary electrons diffuse from the anode column through the negative anode fall. From the continuity equation, at the end of the anode column their intensity is equal to the ion current plus the primary electron losses:

$$I_- = I_+ + I_A K \left(\frac{d}{D}\right)^2 = I_A \frac{1}{\gamma} \left(\frac{d}{D}\right)^2 \left[\left(\frac{m}{M}\right)^{1/2} + \gamma K\right]. \tag{6}$$

Thus, for the usual value of the pressure in the duoplasmatron, the intensity of the secondary electron flux is much smaller than that of the primary electron flux.

The theoretical variation of the charged particle currents as a function of the discharge parameters is obtained from the previous equations, associated with the variations of the secondary parameters of the model γ, L, D, and K, as previously summarized in table 1, Part I.

Inversely these equations have been used[8]) to test the experimental value of γ obtained from electrostatic probe data in the discharge. Furthermore it is the only way to measure the experimental variation of the parameter K characterizing the losses of the primary electron beam travelling across the anode plasma.

An important property may be first proposed: when the arc starvation mode occurs, γ and D suddenly increase, which involves from eqs. (3) and (5), the existence of a maximum of the ion and electron beam currents. The arc current is then [eq. (18), Part I]

$$I_{AM} \simeq en_0 \gamma DL(\pi kT_0/8m)^{1/2}. \tag{7}$$

Thus from eq. (3) the maximum of the ion beam current is

$$I_{+M} \simeq en_0 \frac{Ld^2}{D}(\pi kT_0/8M)^{1/2}. \tag{8}$$

2.2. Influence of the operating parameters

When the source geometry is chosen, the operation with a given gas is described by the values of the pressure and of the electric and magnetic parameters. From table 1 Part I, it appears that the secondary parameters of the model depend only, as a first approximation, on three independent parameters of the discharge: I_A, B and p_A. Thus from eq. (3), one can conclude that the duoplasmatron is a "current generator", the intensity of which depends only on the three parameters above.

We note that when the discharge is operating, the pressure in the cathode chamber is greater than the pressure p_A in the anode chamber. The pressure gradient depends on the arc current and on the magnetic field: it may attain one order of magnitude[8]). Thus a quantitative comparison between experimental data is only possible if one specifies the region where the pressure is measured. Due to the importance of the anode region for determining the discharge and source properties, it seems preferable to measure the pressure in this region – when possible.

2.2.1. *Influence of the extraction voltage*

The current–voltage characteristic of a cooled collector placed just behind the anode aperture is similar to that obtained from an electrostatic probe immersed in a plasma. Two sections with low positive slopes appear, which correspond to the saturation of the electron and ion collection. The latter is obtained when the voltage with respect to the grounded anode, lies between -50 V to -150 V, according to the discharge parameters, and extends to tens of kV. The collected ion current then corresponds to the ion current I_+ flowing through the anode aperture. The duoplasmatron behaves as a "current generator" and as such is only amenable to treatment as a space-charge limited diode operating at saturation. The thickness of the sheath separating the plasma from the collector adapts itself to the Langmuir law. These mechanisms of the extraction of positive ions from a plasma are now well understood[9]). They will not be developed further.

2.2.2. *Influence of the arc voltage*

As shown in fig. 2, the ion beam intensity and the floating potential of the IE are almost independent of the total arc voltage V_A, the parameters I_A, B and p_A being fixed. Under these conditions, the variation of V_A is obtained by varying the cathode heating power P_c. The arc potential has a minimum value when the cathode is overheated and the cathode emission is then space-charge limited. The value of the minimum arc voltage is close to the IE floating potential, because the "cathode fall" potential for space-charge emission is of the same order (5–15 V) as the potential jump between the IE and the cathode plasma [eq. (2), Part I].

Although the arc power is minimum in these conditions, low frequency instabilities are very often generated in the space-charge cathode sheath[10]), which may modulate the emitted ion beam. Thus a judicious choice of the linked parameters V_A and P_c, in order to obtain "temperature" limited emission of the cathode

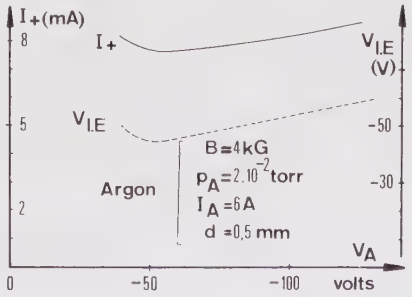

Fig. 2. Dependence of extracted ion current and IE floating potential on total arc voltage V_A.

is necessary to obtain a quiescent source. Furthermore, owing to the higher positive impedance of the arc in this cathode operation, the arc current stability is improved.

2.2.3. *Influence of the IE bias*

In continuous operation of the discharge, the IE may be negatively biased, with respect to the grounded anode, within a broad range extending from a value close to the ionization threshold of the gas down to values more negative than the cathode potential. However, the variation of the IE potential modifies the current repartition between the three electrodes of the structure.

When the IE is floating, the total collected ion current is equal to the total electron current, and the current I_K through the cathode is equal to the current I_A through the anode column. The ions collected by the IE are issued both from the cathode plasma and from the plasmas of the anode discharge, whereas the collected electrons are mainly issued from the more negative plasma, that of the cathode discharge.

Now, when the IE potential is made more negative than the IE floating potential, a net ion current (I_{IE}) is then collected, because the electrons are repelled; but the ion flow is unchanged, as seen from the saturation obtained in fig. 3a, where the current I_A through the anode column is fixed. Because less electrons are lost, the current I_K delivered by the cathode has to decrease in order to satisfy the relation, $I_A = I_K + I_{IE}$. The mechanism for charge collection by the IE is similar to that occuring when a Langmuir probe is placed in a plasma.

In the same manner, when the IE potential increases from its floating value, the electron collection from the cathode plasma increases strongly, whereas the ion collection is almost unchanged, as is observed with a Langmuir probe. However, the cathode current has to increase in order to compensate for the large losses, as shown in fig. 3a. In this range of potential the relation $I_K = I_A + I_{IE}$ is satisfied.

From this discussion, it appears that the current–voltage characteristic of the IE and the resulting variation of the extracted ion current has a physical sense only if one defines which current is maintained at a fixed value. The difference is clearly illustrated in fig. 3a, I_A being constant, and in fig. 3b, I_K being constant. From these graphs, one can conlude:

— When the anode discharge current is constant, the ion beam current is almost independent of the IE bias. This observation is in agreement with eq. (3), as none of the parameters are affected; the ion losses on the IE being almost unchanged, γ remains constant. Only a slight decrease (5–10%) of I_+ is observed when the IE collects electrons. The ion losses in the IE canal are slightly reduced, causing an increase of γ in eq. (3).

— When the cathode discharge current is constant,

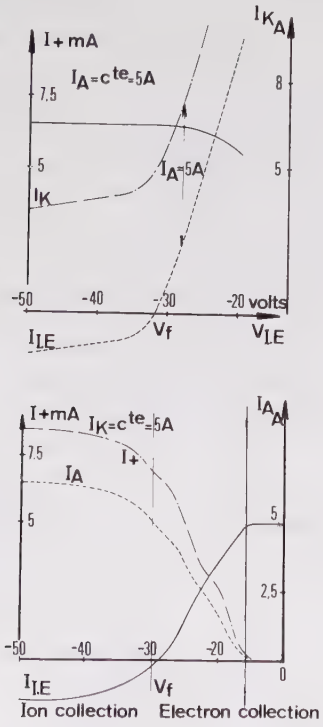

Fig. 3. Influence of the IE bias on I_{IE}, collected current on the IE, I_K, current to the cathode and extracted ion current I_+. a) The current I_A across the anode column is constant. b) The current I_K to the cathode is constant. Argon — $p_A = 2.10^{-2}$ torr, $B = 4$ kG, $e = l = 5$ mm, $D_2 = 7$ mm, $d = 0.5$ mm.

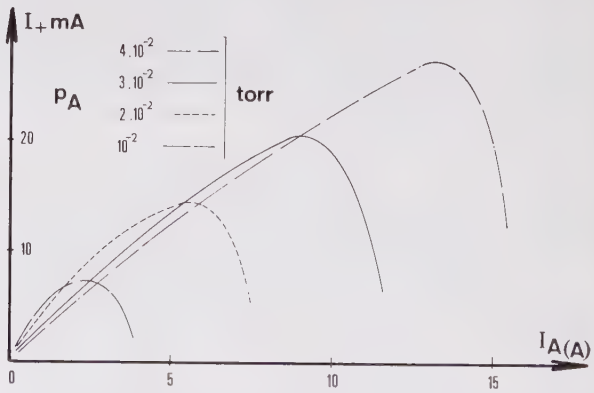

Fig. 4. Dependence of extracted ion current on arc current; anode pressure parameter. For argon $B = 5$ kG; $d = 0.7$ mm; $l = 3$ mm, $D_2 = 7$ mm.

the biasing of the IE modifies both I_A and I_+, but the latter remains proportional to I_A, in agreement with eq. (3).

Thus, the regulation role of the "grid", as is usually understood, is only related to the division of the cathode current between the anode and the IE without modification of the fundamental mechanisms of the anode discharge.

2.2.4. *Influence of arc current, pressure, and magnetic field*

The variation of the extracted ion beam may be summarized as follows for the case of an unsaturated magnetic circuit.

i) *Normal arc mode*

The ion beam intensity is proportional to the arc current (fig. 4), decreases slightly with increasing pressure (fig. 5) and is proportional to the magnetic field strength.

These properties are in agreement with eq. (3), in which $D^2 \sim B^{-1}$, has been experimentally measured. One obtains

$$I_+ \sim I_A B. \tag{9}$$

The slight decrease of I_+ with increasing pressure is related to a slight increase of the column diameter resulting from charge scattering on neutrals.

ii) *Regime-change-over point*

The ion beam intensity is maximum at the regime-change-over point of the arc (fig. 4). As a first approximation, the intensity of the maximum is proportional to the anode pressure (fig. 6) and proportional to the square root of the magnetic field maximum (fig. 7):

$$I_{+M} \sim p_A B^{1/2}. \tag{10}$$

To be more precise we note a slight deviation from the linearity in the variation of I_{+M} and I_{AM} as a function of pressure (fig. 6). This results from the increase of the column diameter in eqs. (7) and (8). In the same way, the I_{+M} variation as a function of B is only correctly satisfied when the aperture diameter is much smaller than the column diameter. For example, in fig. 7, for the higher values of B, the maximum of the ion current is smaller than the value calculated from relation (10) because the compression of the column is too strong. However, application of eq. (4) gives a correct result.

Note: If, with increasing magnetic field, the magnetic circuit saturates, the previous laws may no longer be satisfied. When saturation occurs, a reduction of beam intensity is observed as compared to the previous linear variation (fig. 8). However this variation is in qualitative agreement with eq. (3), because the penetration of the fringing magnetic field towards the geo-

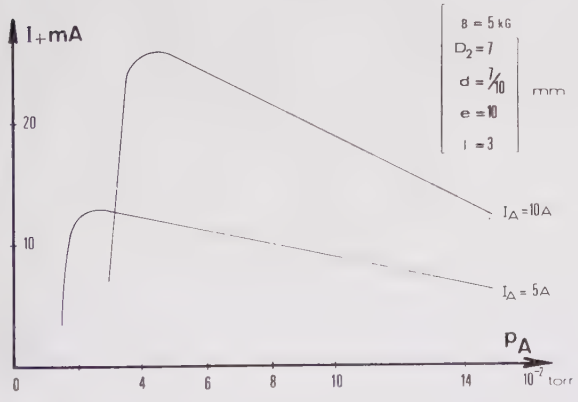

Fig. 5. Dependence of extracted ion current on anode pressure for argon.

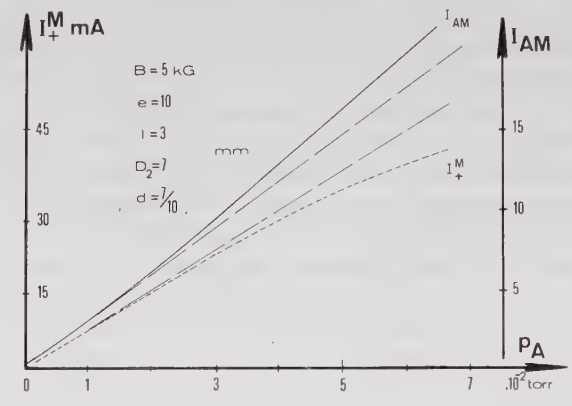

Fig. 6. Dependence of maximum arc current and maximum ion current on anode pressure for argon.

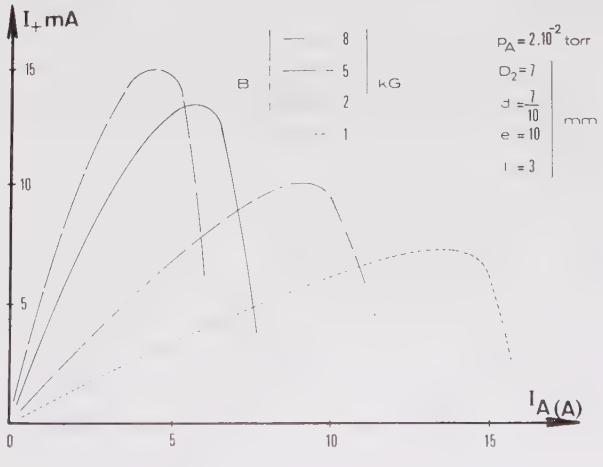

Fig. 7. Dependence of ion current on arc current; magnetic field parameter for argon; unsaturated magnetic circuit.

metric constriction increases, as seen from the experimentally determined magnetic maps. As a result, the ion losses in the IE canal are reduced and γ increases. This example shows the importance of the magnetic field topography. The form and the quality of the magnetic circuit have to be carefully chosen in order to obtain optimal performance of the duoplasmatron.

2.3. Influence of the construction parameters

2.3.1. *Influence of the geometric compression ratio*

The ratio of the diameter D_2 of the IE canal to the diameter D_1 of the cathode chamber has a strong influence on the extracted beam intensity because it determines the operating mode of the discharge. The diameter D_2 and length l_2 of the IE canal have been modified without affecting the magnetic field topography by the addition of non-magnetic pieces inside the canal of a magnetic electrode.

If all other parameters rest unchanged, a reduction of D_2 causes a decrease of the column diameter and consequently (fig. 9) (1) an increase of the extracted ion current and an increase of its maximum [compare with eqs. (3) and (8)] and (2) a decrease of I_{AM} [eq. (7)].

Therefore a decrease of the ratio D_2/D_1, is favorable to obtain a higher energy efficiency. However if this ratio is too small, the "plasma ball" enclosed within the geometric constriction sheath becomes almost spherical in order to insure arc conduction. Coherent oscillations are set up with a frequency of about 100 kHz [10]). Ion beam focus is seriously affected by oscillations at such frequencies. These vibrations result from pseudo-sonor waves excited in the sheath, strongly amplified when resonance conditions are satisfied in the spherical "plasma ball". Coherent oscillations turn into noise if D_2/D_1 increases, the beam modulation being then less than 1%.

Nevertheless, D_2/D_1 must not be too large, because the arc will run without the geometric constriction sheath as explained in Part, I section 2. A magnetic constriction sheath is then set up and the discharge is noisy and the extracted beam is smaller than in a normal mode. The vibrations have the same causes as those observed in the arc starvation mode[10]). Therefore, quiescent source operation is only obtained if D_2/D_1 is properly matched. The empirical optimum value we propose is $D_2/D_1 \simeq 10^{-1}$.

In the same manner, the choice of the IE canal length results from a compromise, because l_2 affects two basic mechanisms of the discharge. With increasing l_2 the ion losses on the canal wall increase, i.e. the extracted ion current increases, as predicted from eq. (3) in which γ decreases. But, if l_2 is too large, the primary electrons issued from the constriction sheath are thermalized over a distance smaller than l_2 and a magnetic constriction sheath is set up. The discharge is then noisy and furthermore a decrease of I_+ is observed. The optimum experimental value is $l_2 \simeq 2D_2$.

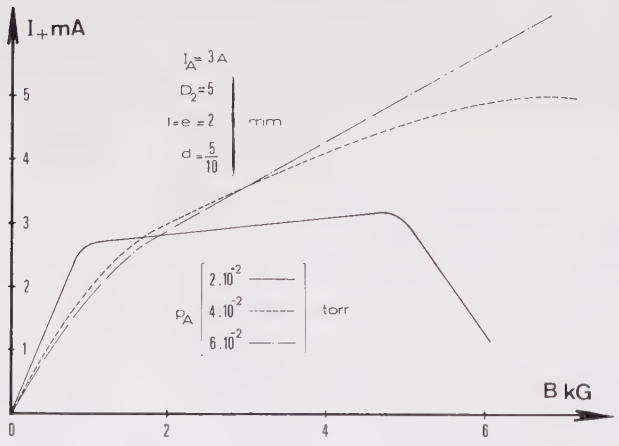

Fig. 8. Dependence of ion current on magnetic field for the case where saturation of the magnetic circuit occurs. Pressure parameter for argon.

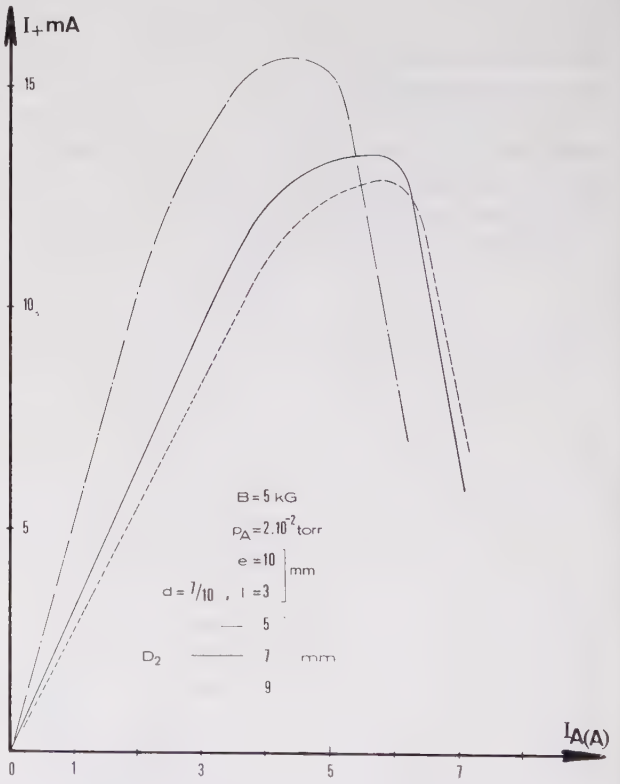

Fig. 9. Influence of the IE canal diameter on the variation of ion current with arc current for argon

2.3.2. *Influence of the cathode position*

The distance l_1 from the cathode to the entrance of the IE canal may be varied over a wide range ($5D_2$–$10D_2$) without affecting the extracted ion current. But, if l_1 is too small, a constriction sheath does not appear and the arc does not run in a normal mode. On the other hand, if l_1 is too large, it is difficult to fire the arc between the cathode and the anode.

The value of l_1 may be matched, within the previous limits, to the ionization mean free path of the gas. Optimal sparking voltage of the arc is obtained, which is important for a pulsed operation[11]).

2.3.3. *Influence of the distance between A and IE*

The distance l between the IE nose and the anode determines the length L of the anode column. As shown in Part I, section 3, this parameter strongly influences the axial potential along the discharge and therefore the regime-change-over point.

According to the magnetic field topography, the measured values of L are equal to l plus several millimeters. The l variation is obtained without affecting the field topography, by increasing the thickness of a molybdenum disc supported by the iron anode. Then, as experimentally tested, the ion losses in the IE canal and the arc column diameter are unchanged. The following results are in agreement with theoretical predictions:

— With decreasing l, $-I_A$, B and p_A being constant – the extracted current is constant, whereas the IE floating potential becomes more negative. Beyond a critical value, arc starvation occurs and I_+ decreases.

— Inversely, the maximum arc current I_{AM} for a normal arc mode increases with increasing l (Part I, fig. 8) as well as the maximum extracted current:

$$I_{+M} \sim p_A B^{1/2} l. \tag{11}$$

The parameter l has the same influence as the anode pressure p_A, and experimental curves, such as those plotted in fig. 4, are obtained.

2.4. Influence of the gas

The influence of the gas on the variation of I_+ as a function of arc current is shown in fig. 10, the arc being far from starvation. It may be seen from this graph that the ion beam current is almost proportional to the square root of the ion mass. A slight deviation is observed for the lighter ions owing to the decrease of the

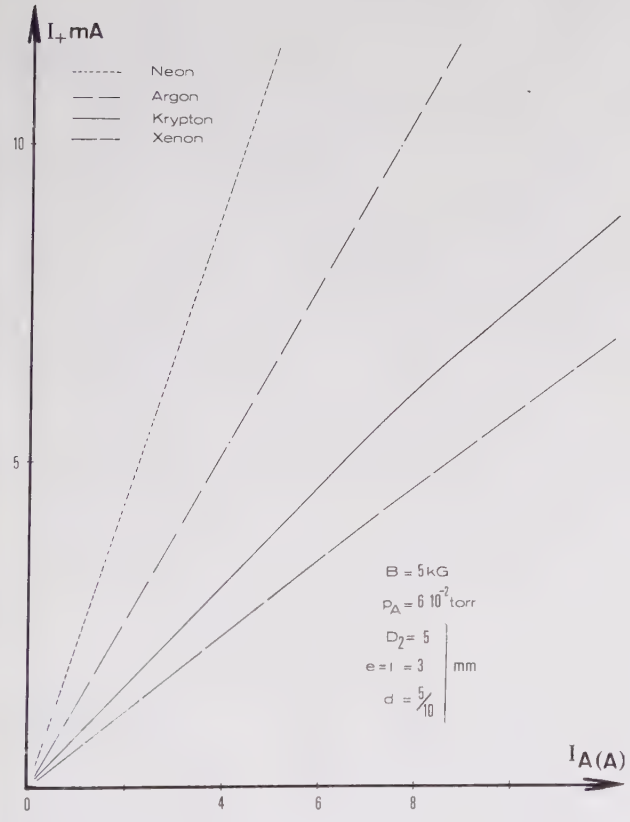

Fig. 10. Influence of the gas on the beam intensity, the arc being far from starvation.

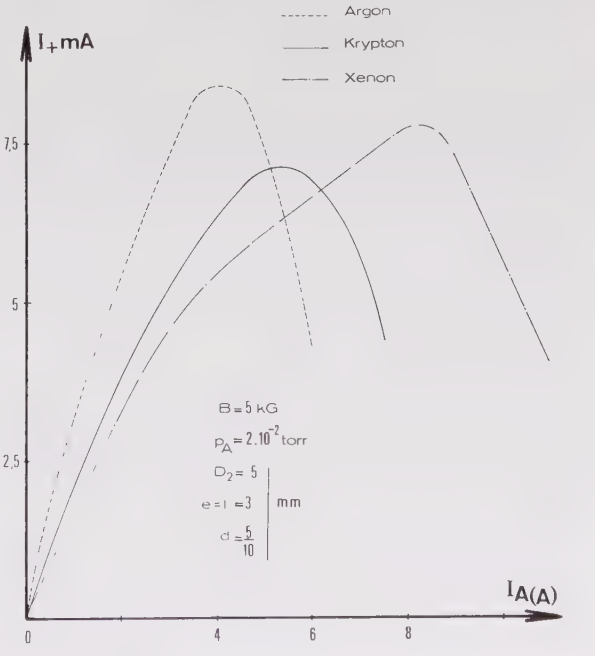

Fig. 11. Influence of the gas on beam intensity and on starvation of the arc.

ion gyroradius causing a decrease of the column diameter [eq. (3)].

Because of the increasing influence of multiply-charged ions as the ion mass increases (section 3), the properties at the regime-change-over point are somewhat perturbed as compared to those derived from eqs. (7), and (8). As shown in fig. 11, I_{AM} increases with increasing ion mass although M is not a factor in eq. (7). The variation $I_{+M} \sim M^{-1/2}$ is also affected. These observations may be explained by a refined model of the discharge, taking into account the influence of multiply-charged ions, which are, in the case of heavy elements, easily produced.

2.5. Summary

Good agreement is observed between experimental and theoretical variation of the extracted ion beam from the duoplasmatron. As a first approximation:

— The extracted ion beam is maximum when arc starvation occurs. The total arc voltage is then of the order of the potential corresponding to the maximum of the cross section for single ionization of the gas.

— The parameters strongly affecting the value of the maximum, causes a variation of the form:

$$I_{+M} \sim p_A B^{1/2} l M^{-1/2} d^2, \tag{12}$$

whereas the corresponding arc current varies as:

$$I_{AM} \sim p_A B^{-1/2} l. \tag{13}$$

— The constants of proportionality in these equations vary slightly from one source to another, and depend on the IE canal dimensions and on the magnetic field topography. Quiescent operation of the source is obtained only if these parameters are properly chosen. Construction criteria have been given.

3. Multiply-charged ion beam production

3.1. Theoretical analysis

Starting from the basical mechanisms of the discharge, we can discuss the optimal conditions for which the duoplasmatron is efficient for multiply-charged ion production and furthermore what is the expected charge distribution.

A rigorous calculation would require the analysis of all the processes which lead to the balance between production and loss for each charge state. Then a more complete discharge model would have to be derived, taking account of the influence of multiply-charged ions on the discharge equilibrium equations. However, the interest of such a model is limited because the atomic parameters of multiply-charged ions are not available with sufficient precision, neither theoretically nor experimentally[12]). Hence, in this paper, the objective will be restricted to present information that should be helpful in understanding the first-order behaviour of the duoplasmatron. They will be derived from a simple approach to the problem, that already used to calculate the charge distribution in a PIG-ion source[13, 14]).

Schematically, the creation of a z-times charged state by electron impact may occur through two basic processes. Firstly the direct ionization of a neutral by single electron impact:

$$A^0 + e \rightarrow A^{z+} + (z+1)e.$$

Secondly, by stepwise ionization: the final charge state is achieved by several successive electron impacts, only one electron being removed at a time:

$$A^{(z-1)+} + e \rightarrow A^{z+} + 2e.$$

In a plasma source, the energy of the ionizing electrons is low. Thus multiple ionization by single impact will provide a rapidly decreasing contribution to higher charge states, because the cross sections decrease strongly with increasing charge multiplicity. On the other hand, the cross section to remove one electron decreases slowly with increasing charge multiplicity. Hence step-by-step ionization is the only method, in such sources, of producing highly-charged ions. However, this process requires that the particles remain in the ionizing region for a time τ-called the ion dwell-time – much larger than the mean time τ' between two collisions in which one electron is removed. The comparison between these two characteristic times provides information about the predominant process. Their value will be derived from the discharge mechanisms and properties discussed in Part I, section 2.

3.1.1. *Ion dwell-time in the anode column*

In the ion free-fall approximation of the discharge model, the ion losses are dominated by the escape to the boundary of the anode column. Volume recombination is negligible as are charge-exchange processes, if the neutral pressure is close to its minimum value corresponding to arc starvation (see below). The ion dwell-time depends on the ion creation point in the column and on the axial variation of potential, which is derived from the plasma-sheath equations for this beam generated plasma[6]). The dwell-time at each

point may be defined by the equilibrium between the uniform production rate G_0 and the escape rate (n_+/τ), where n_+ is the local ion density. A mean value of τ over half of the anode column is obtained by extension of this balance equation to the entire volume:

$$G_0 L/2 = \bar{n}_+ L/2\tau = j_+/e, \tag{14}$$

where $\bar{n}_+$ is the mean ion density over the axial profile of the plasma and j_+ is the ion current density at the anode column boundary. For the case of monocharged ions j_+ is given by eq. (1), whereas $\bar{n}_+ \simeq 0.8 n_{e_0}$. Thus from eq. (14), one obtains the mean dwell-time τ_1 for monocharged ions:

$$\tau_1 \simeq L(M/2kT_e)^{1/2}, \tag{15}$$

which depends only slightly on the operating parameters, through the variation of the secondary electron temperature T_e.

For the case where the space-charge neutrality of the plasma is mainly insured by z-times charged ions ($n_e = z n_{z+}$), the mean dwell-time of these latter is given by:

$$\tau_z = \tau_1 z^{-1/2}, \tag{16}$$

as obtained from the modified plasma equilibrium equations.

A typical value of the anode column length of a duoplasmatron is $L = 5$ mm. Thus for argon with $T_e = 4$ eV, one obtains: $\tau_1 \simeq 1.2$ μs. This time is much smaller than the ion dwell-time in PIG-sources. Pigarov and Morozov[13]) have measured a value between 12–16 μs for a 100 mm ionized column. In this discharge, the 3-times charged ion of argon were optimized. Eq. (16) gives a value (14 μs) in agreement with the experimental one.

3.1.2. *Mean time between successive ionizations*

The ionizing collisions in the anode column result mainly from the impact of the primary electrons (energy eU, current density j_e) on the heavy particles. Thus the collision frequency to remove a single electron from i-times charged ions is:

$$1/\tau_i' = j_e \sigma_i^1/e, \tag{17}$$

where σ_i^1 is the cross section of the process. In this expression, no account is taken of the ionization by secondary electrons, whereas ionization from excited or metastable ion states may be included in the cross-section value. The latter contribution has been shown to be very important by several authors[15,16]). It explains the strong discrepancy between theoretical and experimental values of collision cross sections. These authors conclude that, because of this phenomenon: (1) the cross-section value depends strongly on the excitation state of the ion to be ionized and as a consequence is affected by the variation of the energy of the electrons which have produced the ions; (2) the effective cross section, at its maximum, depends little on the charge multiplicity.

Table 2

Mean time τ' between successive ionizations for typical duoplasmatron parameters. σ_1^1 is the maximum of the ionization cross section for mono-charged ions from the theoretical work of Drawin[17]).

Arc conditions	Ion	$\sigma^1 = \sigma_1^1 \times \times 10^{-16}$(cm^2)	τ' (μs)
$I_A = 16$ A, $B = 5$ kG, $D \simeq 1.4$ mm, $j_e = 10^3$ A cm^{-2}	Ar^{z+}	1.1	1.45
	Kr^{z+}	1.5	1.05
	Xe^{z+}	2.0	0.8

Therefore, a large uncertainty results in the evaluation of the cross section. As a first approximation, we shall consider that the maximum of the cross section is independent of the charge multiplicity. The common value σ^1, will be taken as the theoretical cross section σ_1^1 for ionizing monocharged ions, from the work of Drawin[17]). Typical values of the resulting mean time τ' between successive ionizations are given in table 2.

3.1.3. *Charge distribution through stepwise ionization*

To simplify, we assume that charge exchange and volume recombination are negligible (see below) and that the ions remain in the discharge up to a time τ. Charge escape is not explicitly taken into account in the balance equation.

The variation of the population $N_z(t)$ of the z-times charged ions in the entire volume as a function of time will be derived from the set of equilibrium equations such as:

$$dN_z/dt = (N_{(z-1)} - N_z)/\tau', \tag{18}$$

with the initial conditions:

$$N_z(t=0) = 0 \quad \text{if} \quad z > 1$$

$$N_1(t=0) = N_1(0) = \Phi_0[1 - \exp(-a)], \tag{19}$$

the latter equation is obtained from Part I, eq. (9). The solution is:

$$N_z(t) = \frac{N_1(0)}{(z-1)!}\left(\frac{t}{\tau'}\right)^{z-1} \exp -\left(\frac{t}{\tau'}\right), \tag{20}$$

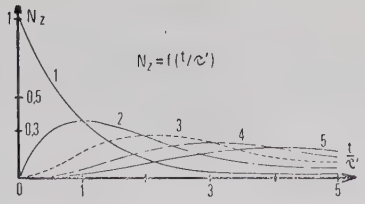

Fig. 12. Calculated variation of the z-times charged ion population with normalized time, as a result of stepwise ionization. τ' is the mean time between two successive ionizing collisions.

the maximum of $N_z(t)$ being obtained when $t = (z-1) \times \tau'$, as shown in fig. (12).

The charge distribution in the particle flux through the anode column ends at time τ is derived from this graph[12]). The most probable charge state z_M being:

$$z_M = (\tau/\tau') + 1.$$

Because of the variation of the ion dwell-time with increasing charge multiplicity [eq. (16)], the most probable charge state lies within the limits:

$$(\tau_1/\tau')^{2/3} \leqslant (z_M - 1) \leqslant \tau_1/\tau'. \qquad (21)$$

3.2. Discussion, experimental results

The discussion of multiply-charged ion production follows from the variation of the ratio τ_1/τ' of the two characteristic times as a function of the discharge parameters:

$$\tau_1/\tau' = \frac{4I_A}{e\pi}\,\sigma^1\,\frac{L}{D^2}\left(\frac{M}{2kT_e}\right)^{1/2}. \qquad (22)$$

3.2.1. *Source with low arc current*

The early duoplasmatrons were built to operate continuously with low values of arc current (< 5 A) and a small distance between the anode and the IE. These conditions correspond to experiments conducted in our laboratory on mercury[18]) and noble gas[3]) as well as experiments reported by Braams et al.[19]).

Typical conditions when arc starvation occurs are given in the first line of table 3. Single electron impact process is important because $\tau_1/\tau' \ll 1$. Its contribution to the production of multiply-charged ions is proportional to the partial cross section from neutrals (σ_0^z). As an example, for argon, taking the experimental cross sections given by Bleakney, the doubly-charged population is:

$$N_2 = N_1(0)\sigma_0^2/\sigma_0^1 \simeq 0.13\,N_1(0) \text{ with } U = U_M = 70\text{ V}.$$

The contribution of stepwise ionization is from eq. (20):

$$N_2 = N_1(0)\,\tau_1/\tau' = 0.1\,N_1(0).$$

The two processes have an almost equal contribution, but the multiply-charged ion production is weak and restricted to the lower multiplicities. For argon, at the regime-change-over point, the experimental abundances in the particle flux are Ar^+: 78%, Ar^{2+}: 20% and Ar^{3+}: 2%. These values agree with those calculated above. This charge distribution depends only slightly on the operating parameters when arc starvation occurs, because the contribution of direct ionization depends only on the gas.

The influence of the discharge parameters is as follows:

— With increasing arc current to I_{AM}, multiply-charged states appear beyond a threshold value of arc current. The threshold increases with increasing charge multiplicity and neutral pressure or with decreasing magnetic field (fig. 13). These results are easily explained from the correlated variation

Table 3

Typical values of the duoplasmatron parameters at the regime-change-over point of the arc, calculated optimized charge state z_M and ratio of electron to neutral density for noble gases.

B (kG)	L (mm)	p_A (10^{-2} torr)	I_{AM} (A)	Ar			Kr			Xe		
				τ_1/τ'	z_M	n_{e_0}/n^*	τ_1/τ'	z_M	n_{e_0}/n^*	τ_1/τ'	z_M	n_{e_0}/n^*
5	3	2	3.6	0.1	1.1	0.3	0.2	1.1	0.6	0.3	1.3	0.75
5	5	2	6	0.3	1.3	0.9	0.6	1.6	1.6	1	2	2.5
5	5	4	12	0.6	1.6	1.8	1.2	2.1	3.6	2	2.6	5
5	10	2	12	1.2	2.1	3.6	2.4	2.8	7.2	4	3.5	10
5	10	4	24	2.4	2.8	7.2	4.8	3.8	14.4	8	5	20
3.6	8	4	18	1.5	2.3	4.5	3	3.1	9	5	3.9	12.5

of the primary electron energy U (Part I, section 3).

Beyond the regime-change-over point, the monocharged ion current decreases abruptly whereas the doubly- and triply-charged ion current increases. An abundance of 60% A^{2+} may be obtained, but the instability level increases and the beam focus deteriorates, as stated previously.

— With decreasing pressure, the electron energy increases to U_M and the multiply-charged ion abundance consequently increases (fig. 14).

3.2.2. *Optimum conditions for multiply-charged ion production*

If stepwise ionization predominates, the charge distribution will be optimized for a charge state z_M higher than unity. If one adopts the less favourable case in eq. 21, z_M is given by:

$$(z_M - 1)^{3/2} = \frac{4I_A}{e\pi} \cdot \sigma^1 \frac{L}{D^2} \left(\frac{M}{2kT_e}\right)^{1/2}. \qquad (23)$$

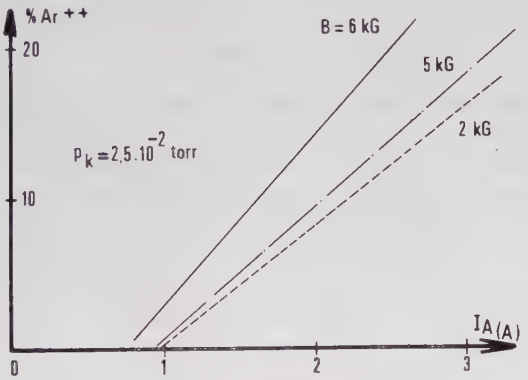

Fig. 13. Variation of doubly-charged ion abundance as a percentage of the total argon particle current, with arc current. Source with small anode column length $l = 1$ mm.

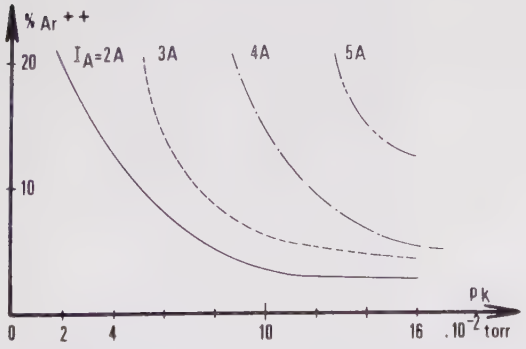

Fig. 14. Variation of doubly-charged ion abundance, as a percentage of the total argon particle current, with cathode pressure. Source with small anode column length $l = 1$ mm.

The conditions necessary to shift the charge spectrum towards higher charge states appear clearly in this expression. Of course, with each set of operating conditions, the destruction processes of multiply-charged ions must be avoided. In a discharge source, for the moderate charge states ($z < 10$), the charge-exchange process is the predominant destruction mechanism, because the cross sections are large – in excess of 10^{-15} cm^2 for low ion velocity[12]). The importance of this process may be evaluated from the comparison of the mean free path for charge exchange $\lambda_{ex} = (n\sigma_{ex})^{-1}$ to the half column length. In particular, when the arc starvation occurs, the neutral density in the arc is minimum and from eq. (15) (Part I), one obtains:

$$\frac{2\lambda_{ex}}{L} = \left(\frac{M}{m}\right)^{1/2} \frac{\sigma_M}{\sigma_{ex}} \gamma\chi \simeq 5, \qquad (24)$$

with $\sigma_{ex} = 5.10^{-15}$ cm^2; $\gamma = 1/5$; $\chi = 3/2$; $\sigma_M = 3.10^{-16}$ cm^2 (argon).

Therefore, charge-exchange processes which involve a decrease of charge multiplicity, will be negligible only if the pressure is lowered to its minimum value compatible with obtaining the desired arc current – i.e. calculated from eq. (7). At the regime-change-over point, the optimized charged state is then also given by:

$$(z_M - 1)^{3/2} = \pi^{1/2} n_0 \frac{L^2}{D} \gamma\sigma^1 \left(\frac{MT_0}{mT_e}\right)^{1/2}, \qquad (25)$$

an expression obtained from eqs. (7) and (23).

Table 3 lists typical duoplasmatron parameters at the regime-change-over point of the arc, and the calculated optimized charge multiplicity z_M, from eq. (23). Also given is the ratio of electron density n_{e_0} to neutral density n^* in the arc column. From eqs. (14)–(17) one obtains:

$$\tau_1/\tau' = \bar{n}_{e_0} \sigma^1 / n^* \sigma_M. \qquad (26)$$

Stepwise ionization predominates only if the plasma is almost fully ionized.

Illgen[11]) and Krupp[21]) have carried out extensive development of a pulsed duoplasmatron for multiply-charged ion production. Their experimental conclusions agree with those derived from our calculation. They may be summarized as follows.

Intense arc current (up to 25 A) are necessary in order that stepwise ionization becomes efficient. This condition, however, is not sufficient: at a fixed pressure, the magnetic field must be matched in order to insure a strong arc constriction, so that the arc goes to or beyond the starvation. This behaviour is illustrated in

figs. 19, 20 of ref. 21. It is explained from the influence of the column diameter in eq. (23). As predicted from eq. 7, the matched magnetic field increases with increasing pressure, for a given range of arc current. Consequently, the optimized charge multiplicity increases [compare to eq. (23)]. The experimental variation of multiply-charged ion population as a function of arc current [fig. 15, from the work of Krupp[21])] is then similar to the calculated variation drawn in fig. 12, the ionizing time τ' being almost inversely proportional to the arc current, and the dwell-time being independent of I_A.

The influence of the pressure is as follows: I_A and B being fixed, the charge spectrum is shifted towards higher charge states with decreasing the pressure. This fact corresponds both to an increase of the primary electron energy and to a decrease of the charge exchange processes.

The energy of the ionizing electrons is not an independent parameter, but depends on the parameters I_A, B and p_A (Part I, section 2). Therefore, when the arc starvation occurs, the energy has a value (eU_M) only dependent on the gas. The maximum optimized charge state is limited by the ionization threshold, although the conditions might be favourable for a further step-by-step ionization. As an example, for krypton, we noted that $U_M \simeq 50$ V. Therefore, in the normal mode, the maximum state will be Kr^{3+}. To obtain Kr^{4+} and Kr^{5+} the arc must run in the starvation mode which is obtained by further decreasing the pressure or increasing the arc current. However, under these conditions, the instability level increases and the beam focus deteriorates. These facts have been observed by Krupp[21]).

Large abundances of multiply-charged ions are only obtained by increasing the distance between A and IE. With $l = 6$ mm, Illgen[11]) obtained the optimization of Ar^{2+}, Kr^{3+} and Xe^{4+}, the other parameters being shown in the last line of table 3. Also are shown the optimized states that we calculated from the model; they are equal to the experimental ones. The optimized experimental spectrum for Kr, from the work of Illgen[11]) is plotted in fig. 16 where the calculated spectrum from the eq. (20), taking $t = \tau = 2\tau'$ is also plotted. The agreement is good if we consider the causes which may modify the charge distribution: (1) the uncertainties in the cross-section values; and (2) the influence of recombination on the wall of the extraction canal. Illgen has experimentally demonstrated that the increase of the canal length causes a destruction of the higher charge states towards the lower ones.

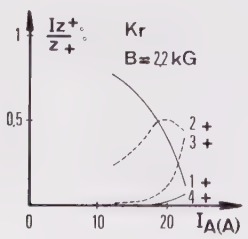

Fig. 15. Variation in percentage of krypton particle current with arc current at matched magnetic field, from the work of Krupp[21]). Stepwise ionization predominates.

3.3. Summary

The duoplasmatron may deliver intense beams of multiply-charged ions, the charge spectrum being optimized at a moderate charge multiplicity ($z_M \leqslant 5$). The source parameters have to be properly matched. Stepwise ionization is then efficient and the simple approach to the problem that we have developed gives agreement with experimental results. The optimized charge state is related to the discharge parameters by the relation:

$$(z_M - 1)^{3/2} \sim I_A B L \sigma^1 M^{1/2}, \qquad (27)$$

the pressure being matched, so that the arc runs near the regime-change-over point. Under these conditions the source is quiescent and high brillance should be obtained. Continuous operation is possible up to 30 A arc current if the cooling system is improved. The lifetime of the cathode remains long, as compared to a

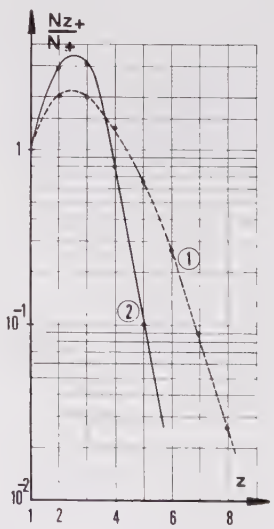

Fig. 16. Charge distribution of krypton particle current: 1) Calculated as a result of stepwise ionization, from eq. (20) with $t = \tau = 2\tau'$. The triply-charged state is optimized. 2) Experimental, from the work of Illgen[11]).

PIG-source, because the energetic ions from the anode column do not reach it.

However, this source is not favourable for the production of higher charge states (up to 10) because they are only obtained in the starvation mode of the arc in which the beam focus is generally perturbed by plasma instabilities.

4. Ionization efficiency

4.1. Theoretical expressions

The ionization efficiency or ion yield is the ratio of the total flow of heavy charged particles to the total flow of heavy particles N_0 through the extraction aperture. In the case of positive ions:

$$\eta = \frac{\Sigma I_{z+}/ze}{N_0}. \tag{28}$$

To derive the first-order behaviour of the source from the discharge model, we neglect the effect of multiply-charged ions, and assume that the neutrals are emitted without interaction with ions. This latter assumption is valid because we have seen that near arc starvation, charge-exchange processes are negligible.

The neutral flow N into the vacuum is then calculated from the neutral density n inside the arc column by the classical effusion law:

$$N = n(kT_0/2\pi M)^{1/2}\pi d^2/4. \tag{29}$$

The total flow N_0 is

$$N_0 = N + (I_+/e),$$

and

$$\eta = (1 + eN/I_+)^{-1}. \tag{30}$$

From the expressions of N and I_+ [eq. (3)], and, taking account of the theoretical eqs. (8), (11) and (12) of Part I, we obtain two equivalent expressions for the efficiency:

$$\eta = \left[1 + 0.7\,\frac{n}{n_{e0}}\left(\frac{T_0}{T_e}\right)^{1/2}\right]^{-1}, \tag{31}$$

or

$$\eta = \left[1 + \frac{1}{2a}\,\frac{D}{L}\right]^{-1}. \tag{32}$$

The former is classical for plasma ion sources[22]). It is useful for the discussion of source efficiency for a given value of the extracted beam. The latter is more convenient for discussion of the influence of the arc modes.

4.2. Discussion and experimental results

The experimental values for the efficiency have been measured under two different conditions: (1) the ions are collected by a probe placed just behind the anode hole; the losses are reduced to the losses on the extraction canal, and the efficiency characterizes the "discharge"; (2) classical extraction is used, followed by a magnetic analysis of the beam composition. The efficiency in then characteristic of the "source+ expansion cup". In both cases, the ion yield values are corrected for multiply-charged ion composition.

4.2.1. *Influence of the arc modes*

In fig. 17 both the experimental values of the ionization efficiency and the calculated values from eq. (32) and theoretical values of the ionization index are plotted. The latter are also plotted on the graph, up to starvation. The agreement is satisfactory. The ionization efficiency of the "discharge" is maximum at the regime-change-over point and decreases in the arc starvation mode because of the increasing diameter of the arc column. Part of the discrepancy between experimental and theoretical values may be attributed to the influence of the losses on the walls of the extraction aperture. Another part of the discrepancy corresponds to the increase of the column diameter in the vicinity of the arc starvation.

The value of the maximum efficiency is close to unity, even for small values of the arc current, allowing continuous operation of the source. Such a high efficiency corresponds to the high ionization degree of the anode column, itself related to the decrease of the neutral density inside the arc column when arc starvation occurs. However, a precise evaluation of this latter phenomenon is not available from the experimen-

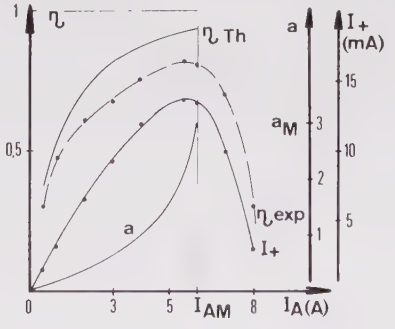

Fig. 17. Dependence of ionization efficiency on the arc modes. η_{exp} – experimental value; η_{th} – theoretical value, calculated from the theoretical variation of the ionization index a and with $D = 1.4$ mm and $L = 5$ mm for argon. $B = 5$ kG, $p_A = 2.10^{-2}$ torr, $d = 7/10$ mm and $l = 3$ mm.

tal variation of the efficiency, because the contribution of ion recombination on the walls is of the same order of magnitude, as the neutral flow issued from the discharge. Thus, the decrease of neutral density as a function of arc current has been studied optically[8]).

The influence of the pressure on the efficiency is discussed simply using eq. (31). I_A and B being fixed, the electron density and beam intensity are almost constant with decreasing pressure, down to arc starvation. The neutral density is then minimum (n^*) and the efficiency is maximum, because, below the minimum pressure, n_{e_0} decreases abruptly. From a practical point of view, it should be noted that the ion energy spectrum varies as the pressure decreases[4]); thus the beam optical properties may also be modified.

4.2.2. *Optimization of the efficiency of the "discharge"*

The maximum possible value of the ionization efficiency may be expressed as a function of the discharge parameters. From the definition of the ionization index a [eq. (14), Part I] one obtains :

$$\eta_M = \left[1 + \frac{eD^2}{I_A L \sigma_{Mz}} \left(\frac{\pi k T_0}{8M}\right)^{1/2}\right]^{-1}. \qquad (33)$$

Therefore, in so far as the pressure is matched so that the arc runs at starvation, the maximum possible efficiency of the "duoplasmatron discharge" will be nearest to unity with:

— increasing the arc current and the magnetic compression – therefore the extracted beam is more intense;
— increasing the arc column length;
— operating with a heavy gas.

Practically, in using the source for the production of an ion beam of a given intensity, the question of the ionization efficiency may be expressed in another way. The carrier density $n_{e_0} \sim I_A/D^2$ must be constant [eq. (3)]. We then conclude from eq. (33) that the maximum possible value of the ionization efficiency is larger the greater the arc column length L. This phenomenon is illustrated in fig. 18, where the theoretical variation of η_M is plotted, for the case of argon, as a function of L for different values of the ion beam intensity. The optimum geometry may be determined from this graph, according to the ion mass and to the expected ion beam intensity. On the other hand, the ionization efficiency of the discharge is closer to unity with increasing ion beam intensity and ion mass, for a given value of the arc column length.

These conclusions are in agreement with those already reported by Almen and Nielsen[23]) for a PIG-geometry with axial extraction and by Chavet[24]) for a Bernas–Nier source with radial extraction. However, in the duoplasmatron, the ionization efficiency of the "discharge" is much higher. When the length of the column is optimized, the ionization efficiency maximum is mainly limited by the ion losses on the aperture wall if a too strong compression of the arc is avoided, compared to the aperture diameter. The practical limitation of the ionization efficiency of the "discharge" is about 90%.

4.2.3. *Ionization efficiency of the "source + expansion cup"*

The presence of the expansion cup has been shown to be necessary in order to improve the optical quality of the intense ion beam extracted from the duoplasmatron. However, the cup causes ion losses depending on its geometry, on its polarization, and on the stray magnetic field of the source[25]).

The influence of a long expansion cup, either insulated from the anode or grounded, is shown in fig. 19. A

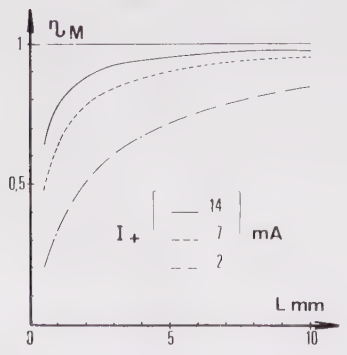

Fig. 18. Dependence of theoretical efficiency, at maximum, on the arc column length, for different values of extracted ion current for argon, $D = 1.4$ mm, $d = 0.7$ mm, $\gamma = 1/3$.

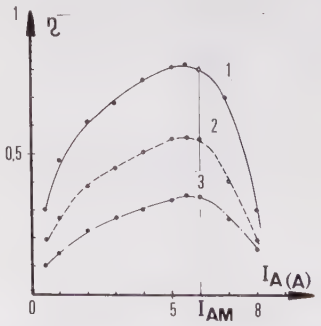

Fig. 19. Influence of an expansion cup on source efficiency. 1) Ionization efficiency of the "discharge". 2) Source efficiency with an insulated expansion cup. 3) Source efficiency with a grounded expansion cup. All other parameters remaining as in fig. 17.

maximum for the efficiency is still observed at the regime-change-over point, but the values are lower as compared to the "discharge efficiency". It appears that an insulated cup provides a better efficiency. Fortunately, this operating condition also gives an improvement of the beam emittance. Gautherin[2]) has shown that a further amelioration of these two properties may be obtained if a weak axial magnetic field ($\simeq 50$ G), created by auxiliary coils, is superimposed on the stray magnetic field of the source in the same direction. However, the magnetic field must be cancelled on the plasma emitting surface. An ionization efficiency close to the discharge efficiency is then obtained, associated with a high value of the brillance.

4.3. Summary

When operating near arc starvation, the ionization efficiency of the duoplasmatron discharge is close to unity if the source construction is properly matched to the expected ion beam intensity. An adequate control of the diffusion of the plasma within the expansion cup allows for the reduction of the ion losses. The efficiency of the "source" is then almost equal to the "discharge efficiency".

5. Conclusion

In source development there is an interaction between atomic physics and plasma physics problems. They affect source characteristics and performances in a fundamental way. The different aspects of the problems occurring in the duoplasmatron source have been analyzed, both theoretically and experimentally. The model of the discharge we have elaborated provide evaluation of the source performance in terms of the ionization and transport processes involved. Theoretical expressions have been derived for the extracted ion current, beam composition and ionization efficiency as functions of the source parameters. These expressions are shown to be consistent with extensive experimental data. Results on the stability of the plasma and emitted ion energy spectrum have been previously reported.

From these results it is possible to determine as a first approximation the optimum values of the construction and operation parameters of the source, according to the requirement of any particular application.

It is a pleasure to acknowledge many fruitful discussions with Professor G. Gautherin and the expert assistance of A. Chabrier with the experimental program. The author is indebted to Dr A. Schlachter who has improved the english in this paper.

References

1) C. Lejeune, Part I of this article, Nucl. Instr. and Meth. **116** (1974) 417.
2) G. Gautherin, Doctoral Thesis, (Orsay, 1967); Nucl. Instr. and Meth. **59** (1968) 261.
3) C. Lejeune and F. Prangere, C. R. Acad. Sci. Paris **265B**, (1967) 389.
4) G. Gautherin, C. Lejeune and A. Septier, Plasma Phys. **11** (1969) 397.
5) M. Dubarry, 3rd cycle Thesis (Orsay, 1972).
6) D. A. Dunn and S. A. Self, J. Appl. Phys. **35** (1964) 113.
7) D. Bohm, in *Characteristics of electrical discharges in magnetic fields*. (eds. A. Guthrie and R. W. Wakerling; McGraw-Hill, New York 1949).
8) C. Lejeune, Doctoral Thesis no. 810 (Orsay, 1971).
9) A. Septier, Proc. Symp. *Ion Sources*, BNL 50310 (Brookhaven, 1971) p. 9.
10) C. Lejeune, Proc. 2nd. Intern. Conf. *Ion Sources*, (Vienna, 1972), p. 387.
11) J. Illgen, UNILAC Report 4–68 (1968).
12) G. Gautherin and C. Lejeune, Proc. 8th Int. Conf. *Mass Separators*, EMIS (Sweden, June 1973).
13) Y. D. Pigarov and P. M. Morozov, Sov. Phys. Tech. Phys. **6** (1961) 342.
14) J. R. J. Bennet, IEEE Trans. Nucl. Sci. NS-**19** (1972) 48.
15) P. A. Redhead, Can. J. Phys. **45** (1967) 1791.
16) Z. Z. Latypov, S. E. Kupriyanov and W. S. Tunitskii, Sov. Phys. JETP **19** (1964) 570.
17) H. W. Drawin, Z. Physik **164** (1961) 513.
18) A. Septier, F. Prangere, H. Ismail and G. Gautherin, Nucl. Instr. and Meth. **38** (1965) 41.
19) C. M. Braams, P. Zieske and M. S. Kofoid, Rev. Sci. Instr. **36** (1965) 1411.
20) W. Bleakney, Phys. Rev. **36** (1930) 1303.
21) H. Krupp, UNILAC Report 1–68 (1968).
22) W. Walcher, *Electromagnetic Isotope Separators* (ed. Koch; North-Holland, Amsterdam, 1958) p. 270.
23) O. Almen and K. O. Nielsen, Nucl. Instr. and Meth. **1** (1957) 301.
24) I. Chavet, Doctoral Thesis, série A no. 17 (Orsay, 1965).